8-2015

Real-time Spectroscopic Analysis of Microalgal Adaptation to Changing Environmental Conditions

Robert Ked Byrd
University of Tennessee - Knoxville, rbyrd18@vols.utk.edu

To the Graduate Council:

I am submitting herewith a thesis written by Robert Ked Byrd entitled "Real-time Spectroscopic Analysis of Microalgal Adaptation to Changing Environmental Conditions." I have examined the final electronic copy of this thesis for form and content and recommend that it be accepted in partial fulfillment of the requirements for the degree of Master of Science, with a major in Chemistry.

Frank Vogt, Major Professor

We have read this thesis and recommend its acceptance:

Tessa R. Calhoun, Robert J. Hinde

Accepted for the Council:
Carolyn R. Hodges

Vice Provost and Dean of the Graduate School

(Original signatures are on file with official student records.)

Real-time Spectroscopic Analysis of Microalgal Adaptation to Changing Environmental Conditions

A Thesis Presented for the

Master of Science

Degree

The University of Tennessee, Knoxville

Robert Ked Byrd

August 2015

Dedication

To Kadie, and my loving family, who have supported and encouraged me throughout this entire process. I would not have succeeded without them.

Acknowledgements

This thesis was supported by the National Science Foundation under CHE-1058695.

Abstract

Increases in anthropogenic pollution are causing many environmental problems; understanding their impact on the environment has become an important issue. Industrialization and the burning of fossil fuels have caused increased levels of carbon dioxide to enter the atmosphere, which is contributing to global warming and ocean acidification. Agricultural runoff has caused levels of inorganic nitrogen and phosphorus to rise, where they have been noted to cause harmful algal blooms. Marine ecosystems have been particularly affected as both of these forms of pollution accumulate in bodies of water. Microalgae are important organisms in these ecosystems because they sequester these pollutants and convert them into biomass. Because the chemical composition of microalgae's biomass depends on the nutrient availability in their environment, further use of microalgae as an *in situ* indicator of environmental conditions is investigated.

The objective of this thesis is to determine how microalgae samples respond in real time to changes in the nutrient availability of their environment. To accomplish this, a novel sensing technique was developed that allowed spectroscopic analysis of live microalgae samples. FTIR spectroscopy in ATR mode was used to repeatedly monitor cells at two distinct carbon dioxide concentrations, standard and elevated, over a twelve hour time period. The change in absorbance over time was modeled nonlinearly to gain information about how the chemical composition of microalgae adapted to higher levels of carbon dioxide. This innovative hard-modeling of changing spectroscopic time series demonstrated the ability to yield interpretable chemical information about the adaptation of microalgae to an altered environment.

Keywords: carbon dioxide sequestration, microalgae cells, FTIR, nonlinear regression, chemometrics

Table of Contents

List of Tables

List of Figures

1. Introduction: Microalgae as Embedded Environmental Sensors

1.1. Objectives

Since the beginning of the industrial revolution, the burning of fossil fuels and other industrial processes have caused carbon dioxide levels in the atmosphere to increase about 43%, with a large percentage of this increase occurring after 1960 [1] - [5]. Many environmental problems have been linked to this increase in carbon dioxide [3] - [5]. As a greenhouse gas carbon dioxide is a major contributor to the current global warming trend. Since 1960, average surface temperatures of the Earth have increased about 0.6 °C (~1.1 °F) [6]. This warming causes the melting of ice caps, which then raises the sea level and causes changes in weather patterns (e.g. El Niño [7], [8]). The sea level has risen about six inches in the past 50 years [9] and this trend is predicted to continue, putting coastal areas at even greater risk [10], [11]. Since atmospheric carbon dioxide partially dissolves into the oceans where it can form carbonic acid [12], increasing carbon dioxide levels translates into an increase in the overall acidity of ocean water [3]. This acidification has been shown to cause coral bleaching [13], [14] and the depression of both metabolic rates in jumbo squids [15] and the immune system response of blue mussels [16].

Moreover, agriculture has led to ‘nutrient pollution’ [17], i.e. the release of excess amounts of nitrates and phosphates into aqueous ecosystems in the form of runoff and leaked sewage. From 1860 to 1990 the amount of reactive nitrogen added to oceans increased by 80% and the current amount of phosphorus being added to the environment has tripled since 1960 [18]. Nutrient pollution causes increased levels of contaminants in drinking water, acid rain, and the formation of harmful algal blooms (HABs) [19], [20]. Often, HABs consume large quantities of dissolved oxygen and thereby kill life in oceans on a large scale. In other cases, HABs produce toxins that can contaminate water supplies [20].

Therefore, marine ecosystems are very sensitive to anthropogenic shifts in their chemical balance. This in return impacts, often in a negative way, the biosphere on which mankind depends.

On the other hand, microalgae utilize these excess inorganic pollutants (carbon, nitrogen, phosphorus, etc.) as nutrients and sequester them into biomass through photosynthesis [21], [22]. For instance, algae account for about half of the Earth's net primary production and sequester more than one hundred million tons of inorganic carbon per year [23]. Since the chemical composition of algae's biomass is affected by changes in its environment [24] - [27], it is mandatory to assess algae's sequestration capabilities to obtain a better understanding of the chemical adaptations they undergo.

1.2. Importance of Microalgae

Algae can be broadly defined as organisms that perform oxygenic photosynthesis and are not a vascular plants [28]. This definition includes both prokaryotic blue-green algae, commonly called cyanobacteria, and eukaryotes. Estimates of the number of species of algae range from 30,000 to 200,000 with ~72,500 being a widely accepted number [28]. Prokaryotic algae lack organelles and are believed to have formed a symbiotic relationship with non-photosynthetic eukaryotic cells that evolved into what are now eukaryotic algae [28]. Algae species can be either multicellular or single celled; some species can be as small as 0.5 µm or as large as 60 m in length [28]. Algae can inhabit marine, freshwater, or terrestrial ecosystems, with marine environments being the most common by far. Some species can survive in severe conditions that most other organisms cannot. Algae of the genus *Dunaliella*, for example, are extreme halophiles that can be found gwowing in salt evaporation ponds [29]. Other species, such as *Galdieria sulphuraria* can grow in water with a pH less than 5 and temperatures in excess of 57 °C [30].

All algae contain the photosynthetic pigment Chlorophyll *a*, which absorbs red and blue light and transmits green light, thus giving green algae their color; some algae contain

additional pigments which give them a different color. Algae in the division Rhodophyta, for example, utilize phycobiliprotein, which gives them a reddish hue. While the shape, size, and preferred environmental conditions may vary from species to species, all photosynthetic algae require inorganic nutrients, (carbon, nitrogen, phosphorus, etc.) sugars, and light to survive [31]. Heterotrophic algae, while not nearly as common as the autotrophic variety, must acquire nutrients from an outside source for their supply of energy [32]. Blue-green algae (cyanobacteria) do not have any sexual reproduction in their lifetime while some species of unicellular and the majority of multicellular algae have a sexual segment to their life cycle [28].

Initially, cyanobacteria were responsible for the oxygenation of the Earth's atmosphere ~2.3 billion years ago [33]. Currently, algae contribute to about half of the global primary production of the biosphere measured as carbon. This process removes carbon in the environment and creates nearly half of the world's supply of O_2 [34], [35]. At least half of microalgal biomass by dry weight is composed of carbon, most of which is derived from atmospheric carbon dioxide [36]. Microalgae are so productive at converting inorganic carbon to biomass that for every 100 tons of biomass produced about 183 tons of carbon dioxide is removed from the atmosphere. This generated biomass then forms the foundation for most aquatic food webs [37]. Algae are also efficient at sequestering other inorganic substances from the environment. They have recently been utilized to treat wastewater and industrial flue gas [31], [38], [39]. By taking advantage of algae's ability to accumulate metals in their environment, some techniques in development use microalgae as a way to recover valuable rare earth metals, such as neodymium, from the environment [30].

In order to take advantage of algae's many commercial benefits, such as their possible use as a source of biofuels [36], they must be grown in such a way that they can be profitably farmed. There are two types of commercial development of algae: open air ponds and closed photobioreactors (PBRs). Open air systems are the simplest method of algal cultivation; they are low in construction cost and easy to operate. These systems require a large area and some form of agitation to ensure algae do not sink to the bottom of the pond. Contamination by other algal species is the largest problem in these open

ponds. To prevent this, cultures with high tolerance for high salinity and pH are grown under extreme conditions. PBRs, on the other hand, allow for a controlled growth environment for the algae that can be tailored to the specific needs of the species; temperature, carbon dioxide, nutrient concentrations, pH levels, and light can all be easily controlled. However, because these are closed systems, buildup of evolved oxygen can occur causing photooxidative damage to the algae and steps to remove the gas must be taken. PBRs are more expensive but can produce much more biomass in the same amount of time as open ponds and can make extraction of biomass easier [34].

Along with PBRs, two techniques have begun to see widespread use in commercial interest of specific compounds produced by microalgae. The first technique takes advantage of the algae's tendency to change its chemical composition and growth rate in response to its environmental conditions [24] - [27]. Algae are first grown in a medium that maximizes their growth rate. Once the ideal amount of algal biomass has been reached, the nutrient medium is altered in such a way to promote the production of the commodity of interest [37]. For example, when *Dunaliella salina* algae grows in medium with high salt content, large amounts of glycerol and β-carotene are produced to help it survive the extreme conditions [29]. Secondly, changes in a cell's genetic code can lead to higher output of commercially significant products by the algae. Genetic manipulation is much more common in cyanobacteria because of their simple DNA structure. Genetic analyses have shown that the gene clusters responsible for producing the macromolecules can be manipulated to increase production or cause the production of completely new compounds. Genetic engineering of blue-green algae of *Synechococcus* sp. has led to its production of the omega-3 fatty acid eicosapentaenoic acid, a substance that it would normally not be able to generate [40].

The development and utilization of these techniques has led to algae becoming a commercially valuable crop. Some of the compounds produced by algae are utilized by the pharmaceutical, cosmetic, and food service industries. *Dunaliella salina* is grown commercially both for its beta-carotene production, which is converted into vitamin A in the human body, and as other dietary supplements [29], [34]. Compounds with anti-inflammatory, analgesic, and antioxidant properties have also been discovered within

microalgae [41]. Humans have used algae as a source of food for thousands of years [42]. They are great sources of proteins and polyunsaturated fatty acids, which are extracted and used in dietary supplements [34]. Red algae are of economic significance as a source of carrageenans and agarose. These compounds are desirable as thickening agents in the food industry and as laboratory culture media [28].

Rising costs and high environmental impact of fossil fuels are leading to research into alternative sources of fuel. Research into utilizing microalgae as one of these alternative fuels has increased recently and its potential is being increasingly recognized. Currently, biodiesel from oil crops and ethanol from sugarcane and corn are being produced in large amounts, but their production is not sustainable [36]. Oil content of some microalgae is greater than 80% of their dry weight of biomass, which is far greater than the percentage of oil crops such as soybean and oil palm, which are less than 5% oil content of biomass. The amount of space needed compared to traditional oil crops is also much less and can be cultivated in areas where traditional farming is unsuitable, which means it will not interfere with production of food crops. Another important advantage of microalgae is that they grow much faster and often double their biomass in twenty-four hours with some species capable of doing so in as little as 3.5 hours [36]. Algae can also be used to produce bioethanol and biogas, such as hydrogen and methane, all of which are carbon neutral [37]. Although the production of algal biofuel is somewhat novel, major steps have been taken to make this technology viable. In 2009, 20,000 gallons of jet fuel produced from algal lipids were sold to the U.S. Navy for $8.5 million and in 2010 the same company sold another 150,000 gallons [43]. It is clear that algae have served and will continue to serve an important role in the environment and as products for human consumption.

1.3. Environmental and Chemical Analyses of Microalgae

Algae have long been used as indicators of environmental health. In the early twentieth century, Kolkwitz and Marsson [44], [45] utilized a technique to assess levels of organic waste in bodies of water called a saprobic system. This non-chemical methodology was based on the number and location of different organisms in streams and rivers, including microalgae. Since that time, the use of algae as indicators of ecological status has thrived [46]. Because of the increased occurrence of algal blooms due to nutrient pollution, the amount of algae in an ecosystem has been used to describe the trophic status of lakes [47], [48]. The responsiveness of many algal species along with their tendency to leave behind certain cell wall components, such as diatom frustules, has allowed researchers to evaluate issues tied to acid deposition and to determine if the rates of acid deposition in lakes has been boosted anthropogenically [49], [50]. Today, government agencies in many parts of the world use algae to observe and evaluate environmental conditions in aquatic ecosystems [46].

Since large quantities of marine microalgae species are distributed throughout all oceans, they are highly relevant contributors to compound transformation from inorganic compounds to organic biomass. This ecological relevance has led to in-depth studies of biochemical processes ongoing within individual cells. For instance, Giordano and Bowes [51] studied the carbon allocation in *Dunaliella salina* cells depending on both their type of nitrogen source, nitrate or ammonium, and the carbon dioxide concentration available to them. They found that cells grown with NH_4^+ instead of NO_3^- as their nitrogen source were up to 17% larger but had similar growth rates. Their starch and glycerol content was reduced while many proteins and photosynthetic pigments increased in activity. This is an indication that more carbon was allocated to the proteins under NH_4^+ growth. They also showed that cells grown with carbon dioxide gas rather than high concentrations of dissolved carbon were smaller, and had less protein, starch, and glycerol content while pigment content stayed the same.

Because of the relatively low levels of inorganic carbon in their environment, aquatic algae developed more sophisticated pathways of carbon fixation than terrestrial plants. To aid

their sequestration process, algae employ a CO_2-concentrating mechanism (CCM) that maintains higher internal carbon dioxide concentrations than achievable solely by diffusion into the cell. This facilitates more dissolved inorganic carbon (DIC) becoming accessible to the carbon-fixing enzyme, Rubisco. Other studies investigated how different nutrient availability and light levels affect the CCM. Beardall et al. [52] examined what role nitrogen availability played in the regulation of the CCM. For this purpose, *Chlorella emersonii* and *Gloeomonas* sp. were grown under conditions where inorganic nitrogen was the growth limiting nutrient. The authors found that less nitrogen availability corresponded with lower growth rates. Decreasing growth rates in turn caused steady declines in both the activity of Rubisco and the cellular protein concentrations. Photosynthetic rates, however, remained fairly consistent until the lowest nitrogen levels were reached [52].

Other studies analyzed the effect of various parameters on the CCM and overall photosynthetic rate. The effects of nitrogen source, light, sulfur limitation, iron availability, and phosphorus limitation on the CCM have all been investigated [53] - [57]. More recently, Beardall et al. [58] examined how elevated levels of gaseous carbon dioxide and increased temperatures impacted the photosynthetic rate of microalgae. Photosynthetic rates of five species increased when the concentration of carbon dioxide was increased from 360 ppm to 1800 ppm. The authors also noted that increased global temperatures had multiple effects on microalgae. Higher temperatures results in lower solubility of carbon dioxide in water, resulting in less available inorganic carbon for algae. Warmer temperatures also lead to a decrease in carbon dioxide affinity in the carbon fixing enzyme, Rubisco, and could lead to water temperatures reaching levels out of the preferred range of particular microalgal species [58].

Hays et al. [59] reviewed the changes in community species composition, abundance, and distribution brought on by the changing climate along with the potential socioeconomic impacts that changing algal populations could cause. Over the past forty years, some groups of warm water microalgae have moved 1000 km further north into the Northeast Atlantic Ocean. As these groups of algae move or cease to exist in certain areas, it affects the organisms that are at higher levels in the food web, such as organisms

that are fished commercially. For instance, a decline in commercial catches of anchovies off the Peruvian coast was linked to a decline in zooplankton that use microalgae as their food source [59]. Long term tracking of phytoplankton abundance and range are well documented and, in turn, has led the author to conclude that worldwide monitoring of phytoplankton can be used to predict future changes in marine ecosystems [59].

Although the study of biological and ecological systems serves an important role in algae's utilization as environmental sensors, chemical analyses of microalgae have also been performed often.

One technique that has been used to analyze the chemical composition of microalgae is high-performance liquid chromatography (HPLC). This technique has been used many times in the analysis of pigments contained in the algae cells. Liu et al. [60] employed this technique to investigate the pigments of organisms that contribute to HABs off the coast of China. Thirty-one species were isolated from coastal waters and were analyzed using HPLC to determine their pigment content. The amount of pigment determined by HPLC was then divided by the volume of the cell for each particular species to generate pigment densities. All pigment data was then normalized to the total chlorophyll *a* density to yield a characteristic pigment profile for the algal strains. These pigment profiles were paired with CHEMTAX, a piece of software developed in MATLAB [61], to perform identification of the algae. The authors finally reported that unlike the traditional microscopy techniques used for algal identification, the HPLC-CHEMTAX technique could allow for cellular identification at taxonomic levels lower than class, which is relevant for observation of HABs [60].

X-ray techniques have been used to measure the concentration and accumulation of nutrients in microalgae. Particle-induced X-ray emission (PIXE) [62] was used by Iwata [63] to determine the concentrations of inorganic trace elements contained in the algae and the bioaccumulation rate of one of these elements, zinc. Two types of microalgae were studied, *Nannochloropsis sp.* and *Phaeodactylum sp.* and fifteen elements were determined from the generated X-ray spectra. The trace element analysis required a small volume, 5 mL, and only required fifteen minutes of irradiation time. The author also demonstrated how the technique could be used to study the uptake rate of inorganic

compounds in the algae's environment. Known amounts of Zn^{2+} were added to the cells' culture medium for eighteen hours but PIXE analysis showed that the concentration of Zn in the algae plateaued after six hours [63]. The small amount of sample and short analysis time could make this technique useful for quick identification of algal species present in an ecosystem based on the concentrations of trace inorganic compounds present, but no information can be gained on important organic compounds contained within the microalgae, such as lipids and proteins.

Huang et al. [64] performed Raman spectroscopy analysis of *Chlorella sorokiniana* and *Neochloris oleoabundans* grown under nitrogen depleted and replete conditions. Raman spectra were taken of algae under these two sets of conditions. It was reported that Raman signals due to lipids, particularly triglycerides, were distinctly seen in nitrogen depleted samples of both algae species but not in samples cultured in the nitrogen replete conditions. Signals originating from carotenoids, however, were seen in both depleted and replete nitrogen conditions. The authors also used this technique to perform chemical mapping of lipids and carotenoids in the cell. Raman images were taken and each pixel was filtered for the wavenumber region of the particular compounds. Pixels were then assigned colors based on the intensity of the band of interest; black was assigned to low intensity, red to medium intensity, and yellow to high intensity. Regions rich in lipids and carotenoids were then easily discernable in the final colored image. The ability of this technique to quantify and locate lipids in microalgae cells could prove useful to determine a rough estimate of nitrogen conditions in the algae's environment, but the samples' fluorescence background blocked relevant wavenumber regions which, in combination with photobleaching of cells caused by the intense laser, limited the sensitivity and selectivity of this technique [64].

Fourier transform infrared (FTIR) spectroscopy applied to microalgae samples was found to be particularly useful because of its sensitivity to a wide range of biologically relevant analytes [65] - [69]. This technique can also be performed *in situ* [70], is non-destructive, requires limited amount of sample, and is fast enough for time-resolved analyses of biological processes. When FTIR analysis is performed on microalgae cells, the resulting spectra contain information about their chemical composition [71]. The

chemical composition of different algal species are often similar but the small differences can be detected through the use of FTIR. Because of these spectral discrepancies, FTIR has been used as a means to identify microalgal species [72].

Giordano et al. [24] have applied FTIR to investigate how the chemical composition of microalgae cells shifts according to the nutrient availability. Cells of *Chaetoceros muellerii* were grown in nitrogen depleted and excess environments; in this study, two nitrogen sources, i.e. NH_4^+ or NO_3^-, were utilized. FTIR spectra of cells grown in NH_4^+ had protein bands that were 20-30% higher in intensity than the same bands of cells provided with equivalent NO_3^- concentrations as the nitrogen source. Upon the transfer of cells that had been grown in a nitrogen excess environment to one of depleted nitrogen, the same protein bands decreased in intensity while lipid bands increased. When cells grown in nitrogen depleted conditions were transferred to nitrogen rich growth media, these trends reversed and the protein bands increased in intensity while the lipid band decreased [24].

FTIR studies of microalgae have also been coupled with a novel nonlinear chemometric method, called Predictor Surfaces [25], to utilize three saltwater microalgae (*Dunaliella salina*, *Dunaliella parva*, and *Nannochloropsis oculata*) as environmental probes for quantifying nutrient concentrations. For calibration purposes, each species was grown under different concentrations of inorganic carbon, nitrate, and ammonium, respectively. The relationship between nutrient availability and the microalgae's spectroscopic signature was found to be highly nonlinear. Based on their spectroscopic signatures, concentrations of nutrients in the algae's growth environment were predicted using both the Predictor Surfaces and principal component regression (PCR). Even though PCR is a linear regression technique, it has been used to model some nonlinear effects [73], [74]. It was demonstrated that Predictor Surfaces predicted nutrient concentrations more accurately and more precisely than PCR [25].

Water content in algae cells proved to be a challenge for FTIR analysis of microalgae. For this reason, drying the algae cells prior to IR-spectroscopic analyses has become the standard method; however, this sample preparation step not only voids attempts to study live cells, it may also falsify the biomass' chemical composition by removing volatile

compounds. Keeping cells alive is key for monitoring the cells adaptation to changing environmental conditions.

1.4. Thesis Overview

The objective of this thesis is to utilize the chemical changes that microalgae undergo as an indicator of the chemical state of its aquatic ecosystem. This research project examined these changes through the use of novel spectroscopic and chemometric analysis.

After an overview of current uses and investigations involving algae, the following section of this thesis describes the method by which microalgae samples were prepared for chemical analysis and how this analysis was performed. Chemical analysis of algae cultures was performed through a novel application of FTIR spectroscopy in attenuated total reflectance (ATR) mode, which provided a means for the examination of live microalgae cells. To determine the effect of a changing environment on microalgae cells, samples were exposed to two sets of simulated environmental conditions.

The next section describes a novel chemometric modeling technique which has been developed to derive insights into processes that occur as algae adapt to a shifted chemical environment. The results of this chemometric analysis of acquired spectral data are then presented and compared to identify how alterations in the algae's nutrient availability affected the chemical composition of its biomass. From these comparisons, conclusions were made about how the chemistry of microalgal biosediment changes as it adapts to changes in the simulated environment.

2. Preparation of Algal Cultures for Spectroscopic Study

2.1. Introduction

In order to gain a better understanding of how anthropogenic pollution affects the environment, microalgae's chemical adaptation to shifting environmental conditions has been investigated. For this purpose, algae cultures must be grown under well-defined ambient conditions. Carbon dioxide levels in the simulated atmosphere were altered to study the effect of changing nutrient concentrations. To assess the carbon dioxide induced changes in algal chemistry, FTIR-ATR spectroscopy was chosen because of its ability to sense live cells, the wide range of biologically relevant detectable compounds, its analysis speed in comparison to the cell's processes, and the limited sample prep required to make analyses.

2.2. Growth of Algal Cultures

Limiting contamination of other similar microorganisms, such as bacteria, is important to obtaining reproducible biological samples. Therefore, before growth of algae cultures began, glassware and utensils were decontaminated and prepared for contact with the samples. All flasks and stock bottles were first cleaned with Contrex AP powdered labware detergent (Fisher Scientific), flushed multiple times with deionized water, and set aside to dry overnight. After drying completely, Erlenmeyer flasks were stuffed with a cotton plug (Figure 1), which later provided sterile air exchange for algae cultures, and finally covered with aluminum foil.

Figure 1. (top) Newly inoculated cultures. (bottom) Cultures in exponential growth phase.

Dry, one liter PYREX media storage bottles were then used to prepare the selected growth medium for microalgae cultures, called enriched seawater, artificial water (ESAW) [35], [75], [76]. This medium is suitable for a wide range of marine microalgae and the concentration of nutrients within can be easily manipulated. ESAW was prepared according to the conditions described in reference [76]. A large portion of ESAW is composed of two salt solutions containing anhydrous and hydrous salts, designated as salt solution I and salt solution II, respectively [75]. Salt solution I was prepared by dissolving the compounds listed in Table 1 in enough deionized water to produce 600 mL of solution, which was then transferred to a one liter stock bottle. Salt solution II was created in a similar manner but with the reagents listed in Table 2 and only 300 mL of deionized water; this was also added to the stock bottle containing salt solution I. Once the two salt solutions were combined, nutrient stock solutions were added. Each nutrient stock solution was prepared previously and contained the amounts listed in Table 3 dissolved in enough water to make one liter. One mL of nitrate stock, one mL of phosphate stock, two mL of silicate stock, and one mL each of metal stock I and II were added to the stock bottle containing the two salt solutions. Next, to ensure that the pH of the ESAW remained at 8.2, ten mL of 1M tris-hydrochloride solution (Fisher Scientific) were added to the stock bottle. Eighty-three mL of deionized water were then added to bring the volume to 999 mL before the final sterilization process.

Once flasks were plugged and stock bottles were filled, they were ready to be sterilized. Items were autoclaved [35] (Getinge Vacuum/Gravity Steam Sterilizer, 733LS) for forty minutes at 121 °C temperature and 2 atm steam pressure. Any beakers or pipets used to culture microalgae were also included in this sterilization. All items were marked with autoclave tape to ensure they had been exposed to the correct temperature. After this process, all sterilized medium had to cool for twenty-four hours before the vitamin stock solution could be added. The vitamin stock could not be added before autoclaving; the temperature would have caused its contents to precipitate. Nonetheless, the vitamin stock was separately filter sterilized with a mixed cellulose filter (Fisher Scientific) featuring a pore size of 0.22 µm. This step takes place in an AirScience Purair VLF laminar flow cabinet to ensure sterilization. After filtration, one mL of vitamin stock was added to the now autoclaved ESAW to bring the volume of the final solution to one liter.

Table 1. Reagents used in salt solution I of ESAW [35].

Reagent	Mass (g)	Final Concentration in ESAW
NaCl (Fisher Scientific)	21.19	363 mM
Na_2SO_4 (Fisher Scientific)	3.55	25 mM
KCl (Fisher Scientific)	0.599	8.04 mM
$NaHCO_3$ (Fisher Scientific)	0.174	2.07 mM
KBr (Fisher Scientific)	0.0863	725 µM
H_3BO_3 (Fisher Scientific)	0.023	372 µM
NaF (Fisher Scientific)	0.0028	65.7 µM

Table 2. Reagents used in salt solution II of ESAW [35].

Reagent	Mass (g)	Final Concentration in ESAW
$MgCl_2 \cdot 6H_2O$ (Fisher Scientific)	9.592	41.3 mM
$CaCl_2 \cdot 2H_2O$ (Fisher Scientific)	1.344	9.14 mM
$SrCl_2 \cdot 6H_2O$ (Acros Organics)	0.0218	82 µM

Table 3. Nutrient stock solutions for ESAW medium [35].

Nutrient	Reagent	Mass (g)	Final Concentration in ESAW
Nitrate	$NaNO_3$ (Fisher Scientific)	46.7	549 µM
Phosphate	$NaH_2PO_4 \cdot H_2O$ (Fisher Scientific)	3.09	21 µM
Silicate	$Na_2SiO_3 \cdot 9H_2O$ (Sigma-Aldrich)	15	105 µM
Metal Stock I	$Na_2EDTA \cdot 2H_2O$ (Sigma-Aldrich)	3.09	6.56 µM
	$FeCl_3 \cdot 6H_2O$ (Fisher Scientific)	1.77	6.56 µM
Metal Stock II	$ZnSO_4 \cdot 7H_2O$ (Fisher Scientific)	0.073	254 nM
	$CoSO_4 \cdot 7H_2O$ (Fisher Scientific)	0.016	5.16 nM
	$MnSO_4 \cdot 4H_2O$ (Alfa Aesar)	0.54	2.42 µM
	$Na_2MoO_4 \cdot 2H_2O$ (Acros Organics)	1.48×10^{-3}	6.1 nM
	Na_2SeO_3 (Sigma-Aldrich)	1.73×10^{-4}	1 nM
	$NiCl_2 \cdot 6H_2O$ (Sigma-Aldrich)	1.49×10^{-3}	6.3 nM
	$Na_2EDTA \cdot 2H_2O$ (Sigma-Aldrich)	2.44	8.29 µM
Vitamin Stock	thiamine-HCl (Fisher Scientific)	0.1	297 nM
	Biotin (Fisher Scientific)	0.002	4.09 nM
	Vitamin B_{12} (Fisher Scientific)	0.001	1.47 nM

Microalgae cultures were then grown using the sterilized flasks and culture media. An initial culture of *Dunaliella salina* (#LB200) was provided by The Culture Collection at the University of Texas, Austin (UTEX) [29], [77]. *D. salina* was selected for its simple growth requirements, tolerance for a wide range of nutrient conditions, and its significance as a producer of β-carotene and lipids for pharmaceuticals and algal biofuel [29], [34]. About 15 mL of culture were received suspended in Erdschreiber's [35], [78] medium. Upon arrival, the culture was placed in the laminar flow cabinet, its cap was slightly loosened, and air exchange was allowed to take place before initial inoculation. Before transferring the new culture from its initial vessel, the cap was removed inside the flow hood and the top of the vial was flamed via Bunsen burner to remove possible contaminants. To begin the transfer of the initial culture to its new medium, 50 mL of ESAW were added to a sterile 125 mL Erlenmeyer flask, which was flamed before and after this addition. Using a Finnpipette adjustable volume pipette (Fisher Scientific) and a previously autoclaved pipet tip, two mL of initial culture were transferred from their original vial into the Erlenmeyer flask. The flask was finally flamed and the cotton plug was reinserted. The newly inoculated culture was then placed into a growth chamber (Precision 818, Thermo Scientific) where temperature and light were controlled. The chamber was set to operate at 20 °C with an alternating twelve hour light and dark cycle.

From this initial culture, two types of samples were generated: backup cultures and replicate sample cultures. The purpose of backup cultures was to ensure that the microalgae remained alive over a long period of time; this was accomplished through the use of batch culturing. Cultures produced through batch culturing are allowed to reach all three phases of growth: initial, exponential, and stationary. To carry out this process, a small volume of algal suspension is removed from a mature culture, either in the exponential or stationary phase, and is transferred to a source of fresh growth medium. For this particular study, two mL were removed from the initial culture after one week and transferred to 50 mL of ESAW in a new sterile beaker. Batch culturing occurred weekly by removing two mL of the most recent culture and transferring them to fresh ESAW. All backup cultures were kept for at least three weeks before being disposed. This ensured that if a transfer of algae to fresh media failed for any reason, the process could be repeated from the previous week's culture.

The establishment of backup cultures, along with any other inoculation, was carried out in the aforementioned laminar flow cabinet. This cabinet decreases the amount of particulate matter in the air and allows for ultraviolet sterilization of all surfaces and items that may come in contact with the algae. An ultra-low penetration air (ULPA) filter and a down-flow air circulator also contributed to the reduction of contaminants entering the work area. All surfaces were cleaned with a 70% ethanol solution. Gloves were also wiped with 70% ethanol and worn at all times during the inoculation process.

Replicate samples were the second type of culture to be produced. These samples were used for spectroscopic analysis and were subjected to different growth conditions than the backup cultures. While batch culturing is useful for keeping a species alive over a long period of time or for studies on algal growth dynamics [35], [79], it is limited in its ability to successfully simulate the environment algae experience in a non-laboratory setting. This is because algae are continuously reducing the amount of available nutrients in their environment. By the end of the growth cycle in cultures prepared via the batch method, nutrients become scarce and the cells become environmentally stressed, which alters their chemical composition. Another problem experienced in batch culturing is that as the cells continue to multiply, their cell density becomes so high that self-shading occurs and some cells receive limited amounts of light. To produce more realistic environments for algae, a system of semicontinuous culturing was developed. Semicontinuous culturing is a modification of batch culturing in which the medium is repeatedly diluted to both replenish spent nutrient and keep cell densities from reaching levels that could cause self-shading. This process also keeps cells in the exponential growth phase, where the growth rate is consistent from day to day [35].

For this particular semicontinuous method, nutrients were replaced in two ways. First, growth medium was diluted by removing algal suspension and replacing it with fresh ESAW. Secondly, a simulated atmosphere for the microalgae was created that allowed precise control of the carbon dioxide levels to which the cultures are exposed. This method helps to replace spent nutrient and better simulates a natural environment.

Replicate samples were first inoculated by taking two mL of algal suspension from the most recent backup culture and transferring them into 100 mL of ESAW in a 250 mL

Erlenmeyer flask. All replicate samples were allowed to grow for eight days to ensure they had entered the exponential growth phase and that an acceptable level of biomass had accumulated for spectroscopic study (Figure 1, bottom). The relatively constant growth rate in this phase also enabled a consistent replacement volume for the samples. Removing too little will lead to many of the same problems experienced with batch culturing. Removing too much, on the other hand, will dilute the samples and cause the algae's cellular concentration to be too low for spectroscopic analysis. For these reasons, it was found that the removal and replacement of 20 mL of algal suspension with ESAW was an acceptable volume for this process. This process occurred once a day and was carried out in the laminar flow cabinet, following all previously established guidelines for limiting decontamination. All replicate samples underwent at least five days of liquid nutrient replenishment to ensure acclimation to their new environment before usage for any spectroscopic analysis.

The second replenishment strategy was accomplished by taking advantage of important relationship that carbon dioxide shares with inorganic carbon in aquatic ecosystems. The amount of gaseous carbon dioxide that dissolves in the ocean depends on the concentration of carbon dioxide in the air, temperature, atmospheric pressure, and the salinity of the water in which the carbon dioxide is dissolving into. However, this concentration can be readily calculated if these parameters are known [12]. Aqueous carbon dioxide is part of a chemical equilibrium as described in equation (1):

$$CO_{2(aq)} + H_2O \leftrightarrow H_2CO_3 \leftrightarrow HCO_3^- + H^+ \leftrightarrow CO_3^{2-} + 2H^+$$

(1)

Although dissolved carbon dioxide can exist as H_2CO_3, carbonic acid, the percentage is so small that the concentrations of aqueous CO_2 and H_2CO_3 are typically combined and represented as simply CO_2, leading to equation (2):

$$CO_2 + H_2O \overset{K_1^*}{\leftrightarrow} HCO_3^- + H^+ \overset{K_2^*}{\leftrightarrow} CO_3^{2-} + 2H^+$$

(2)

The equilibrium constants K_1^* and K_2^*, also referred to as the first and second acid dissociation constants of carbonic acid, are temperature and salinity dependent and can be calculated if these two factors are known [12]. Therefore, by knowing the concentration of atmospheric carbon dioxide, atmospheric pressure, temperature, and total salinity in the algae's environment, the concentration of their source of inorganic carbon, HCO_3^-, can be calculated. By keeping temperature, pressure, and salinity as stable as possible and controlling the carbon dioxide that algae experience in the growth chamber, the amount of available inorganic carbon can be controlled and continuously replenished.

Carbon dioxide concentration control was made possible through the use of two mass flow controllers (MFCs) (SmartTrak® 50 Series, Sierra Instruments) (Figure 2A). These instruments allow the flow rate of an incoming gas to be set within a specified range. The two MFCs were in control of supplies of synthetic air and a known concentration of carbon dioxide, respectively. After exiting the two MFCs, the two gases were merged and passed through an extended length of vinyl tubing to ensure sufficient mixing had occurred. The ratio of the two flow rates determined the final concentration of carbon dioxide and could be easily changed to produce a wide range of carbon dioxide concentrations. Once mixed, the gas flow was divided to provide a simulated atmosphere for as many as eight replicate samples. To minimize contamination, each piece of vinyl tubing that was inserted into the cultures' flasks (Figure 1) was wiped down with 70% ethanol as it could not be autoclaved. The carbon dioxide concentration selected for samples in the growth chamber was 289 ppm, the calculated concentration that would generate the same concentration of inorganic carbon described in the recipe for standard ESAW. Cultures began the carbon replenishment the day after inoculation, unlike the ESAW dilution. Three hour gas flow was initiated at the same time as activation of light in the growth chamber, when cells begin to photosynthesize again.

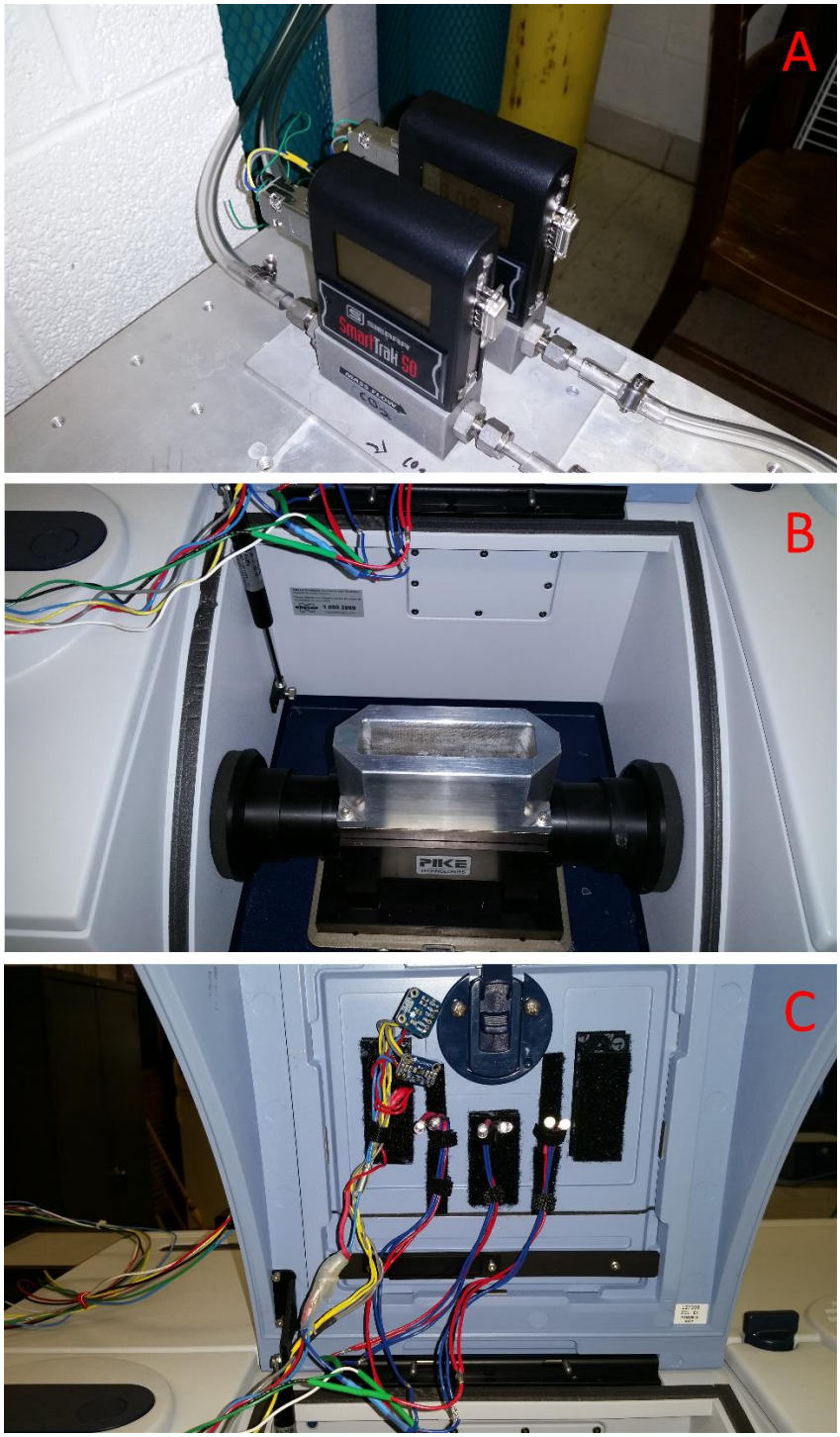

Figure 2. A pair of MFCs used to provide carbon dioxide atmosphere to samples in growth and sample chambers (A). Cultures were transferred into a custom fabricated liquid cell secured atop an ATR apparatus (B) and were illuminated by LED lights placed above the liquid cell (C).

2.3. Chemical Analysis of Live Cells in a Changing Environment

It is important that the spectroscopic technique utilized to analyze microalgae cultures could probe live cells in aqueous media over an extended period of time. By designing the experiment as such, the chemical composition of the microalgae was not falsified in the sample preparation stage and considerable time was saved. The examination of live cells also allowed cells' chemical adaptations to changes in their environment to be observed. It was also essential that this procedure mimicked the simulated environmental conditions of the growth chamber.

This was accomplished by means of FTIR spectroscopy in ATR mode. As IR light passes through the horizontal ZnSe ATR crystal, an evanescent wave is produced and penetrates a small distance, typically from 0.5 to 2.0 µm [80], into sample in contact with the surface of the crystal. By placing an aliquot of algal suspension into the ATR liquid cell (Figure 2B), cells sank to the bottom and deposited onto the crystal surface (Figure 3), where they could be probed by the evanescent IR-field. Once an aliquot of algal suspension was placed in the liquid cell, it and the ATR crystal were placed in a Bruker Vertex 70 FTIR Spectrometer equipped with a DTGS detector (Figure 2B). The FTIR sample compartment was modified to provide light and a simulated atmosphere similar to that of the growth chamber. LED lights were added to the sample compartment and placed so that they would illuminate the liquid algae cell below (Figure 2C). A second set of MFCs was used to also provide a controlled carbon dioxide atmosphere in the sample compartment. Scans were performed on algae in the liquid cell every four minutes for twelve hours. These spectra were recorded with a 4 cm^{-1} resolution and were comprised of 128 co-added scans. Although the instrument scans from 7500 cm^{-1} to 370 cm^{-1}, only the region from 1350 cm^{-1} to 950 cm^{-1} was selected. This region does not overlap with the strong water bands but still contains bands attributed to many biologically relevant compounds.

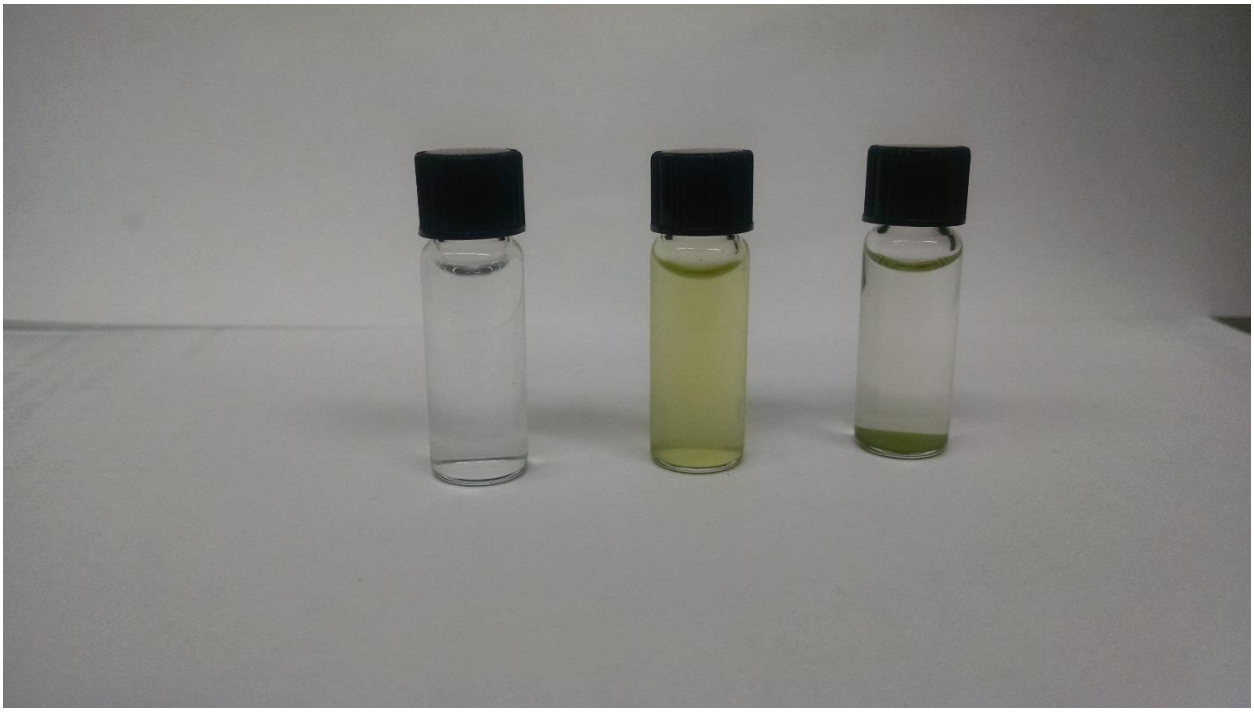

Figure 3. Small vials containing ESAW and *D. salina* algae culture. The left vial contains pure ESAW medium while the other two contain both medium and microalgae. The middle vial has been shaken to suspend the culture homogenously throughout the medium. The right vial contains algae that were left undisturbed for a few days and settled on the bottom of the container.

The period of twelve hours during which FTIR-ATR spectra were recorded was started so it coincided with the beginning of the light cycle in the growth chamber. Thereby, differences in growing conditions in the chamber versus the ATR liquid cell were minimized. In the ATR setup, carbon dioxide was supplied to the cells throughout the entire twelve hours.

During the monitoring period, two processes occur concurrently: (i) algae cells sink and deposit on the ATR cell, where they are probed by the evanescent field, and (ii) due to the chemical shift in their environment, the cells chemically adapt. This leads to two processes contributing to the time-dependent spectral information: the buildup of biomass within the range of the evanescent field and the changes in the chemical composition of cells. To distinguish both impacts on the spectra, two sets of simulated environmental conditions were created in the sample chamber. The first set of simulated conditions samples experienced during the spectroscopic studies was the same as their growth conditions; this established a benchmark. The second set of conditions was designed to trigger and monitor chemical changes within the microalgal biomass in response to a change in their environment. For the duration of this second experiment, microalgae were exposed to elevated levels of carbon dioxide. Using the second pair of MFCs, carbon dioxide levels were increased from 289 ppm, the value provided in the growth chamber, to 1000 ppm, an extreme carbon dioxide concentration that some researchers predict for the year 2100 [81]. The 289 ppm carbon dioxide concentration was calculated to generate ~1.78 mM bicarbonate and the 1000 ppm carbon dioxide provided ~6.18 mM bicarbonate in the culture medium. Due to the design of these two experiments, any differences in the two time series of FTIR-ATR spectra could be assigned to the elevated carbon dioxide level.

2.4. Conclusions

A method of algal culturing was developed to reliably produce samples under well-defined simulated environmental conditions that could be readily altered. Samples were grown under a novel semicontinuous culturing method. In this growth method, inorganic carbon was replenished through control of the carbon dioxide concentration flushed into the headspace of the cultures' flasks; all other nutrients were replenished by replacing a volume of algal suspension with fresh culture medium. These steps provided a culture environment that simulated conditions microalgae naturally experienced more closely than previous methods.

Once cultures became sufficiently acclimated to the semicontinuous technique, they were transferred to a liquid containment cell to undergo FTIR analysis. This cell was sealed atop an ATR crystal so that cells within the algal suspension would sink and form a biosediment on the crystal surface; this allowed live cells to be studied. Samples underwent twelve hours of repeated analysis, with the capture of FTIR-ATR spectra occurring every four minutes. Observed spectroscopic signature changed over time due to more cells joining the biosediment and the algae chemically adapting. To separate these two effects, two sets of conditions were set up for the algae in the sample compartment: a benchmark where the conditions were identical to their growth conditions and a scenario where the carbon dioxide level was increased significantly. MFCs were again used to provide a known concentration of carbon dioxide to the sample compartment to allow an examination of the effects of increased carbon dioxide on the cells' spectroscopic time series.

3. Nonlinear Chemometric Modeling of Spectroscopic Time Series

3.1. Introduction

To gain a better understanding of the chemical adaptations that cells undergo due to environmental change and to utilize the cells as an environmental probe, a chemical model of this system must be established. The chemical processes that occur in biological systems are highly complex. Studies of these processes often find nonlinear relationships between chemical information of significance and measured signals [25]. This nonlinearity can be caused by interactions of analytes in the sample [82] or chemical processes that occur in living samples [83]. Linear techniques, such as PCR and partial least-squares (PLS), can be used to estimate this nonlinear behavior [73], [84], but will not yield any information about the fundamental nonlinear chemical processes that are occurring. For this reason, a novel nonlinear chemometric analysis will be utilized to create a chemical model of the microalgae as it responds to changes in its environment.

The increase in absorbance over time in the spectroscopic time series depicted in Figure 4 is evident. The spectroscopic signature of a given microalgae sample over time depends on the formation of algal biosediment and the chemical reactions occurring in the cells. To describe the generated spectroscopic time series, a model function for the collected experimental data was determined which is comprised of factors relating to the two contributions to measured signal [83]:

$$Y(\tilde{\nu}, t) = A(t) \cdot \varepsilon(\tilde{\nu}, t) \qquad (3)$$

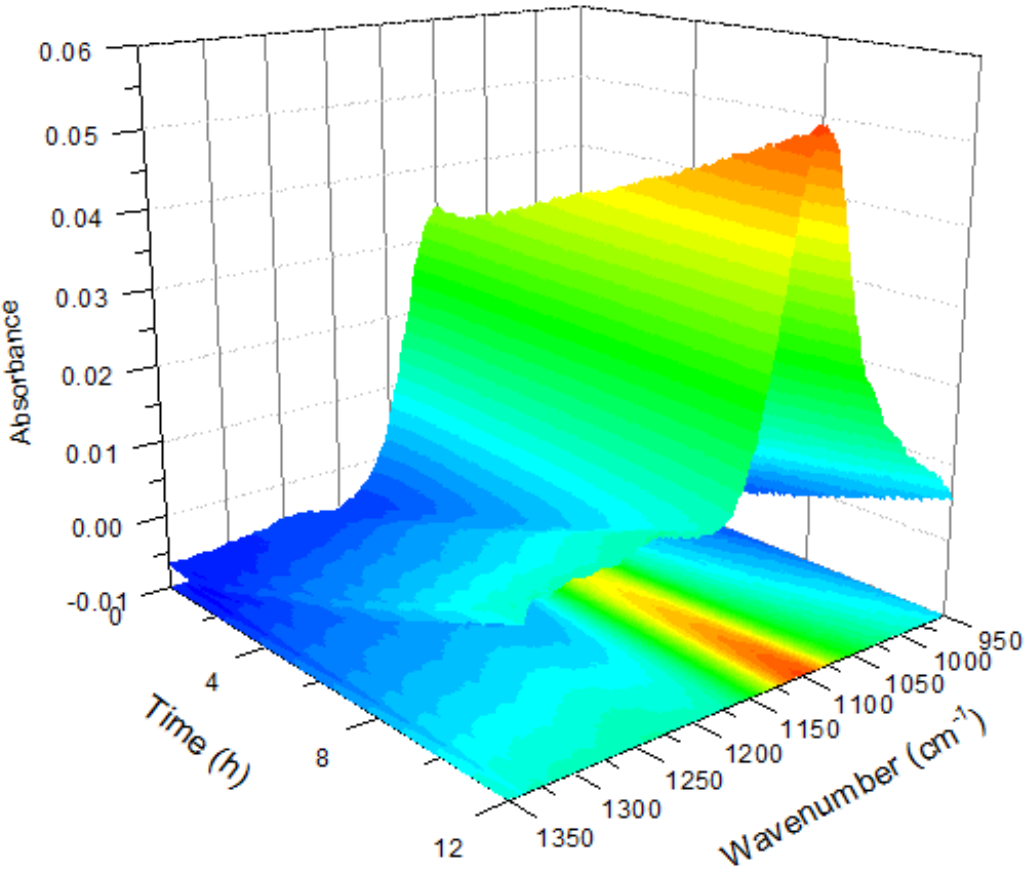

Figure 4. Example of typical spectroscopic time series obtained during a twelve hour analysis period under standard conditions.

The time dependent term $A(t)$ describes the formation of biosediment in the range of the evanescent field and can be considered a time dependent concentration of algal biomass. The other term $\varepsilon(\tilde{\nu}, t)$ expresses spectroscopic components that are dependent on wavenumber and time and thus can model a chemical composition that changes over time. Although $\varepsilon(\tilde{\nu}, t)$ is the only chemically relevant term, the spectroscopic time series cannot be successfully analyzed without incorporating an increase in biomass accumulated within the reach of the evanescent field. The function $\varepsilon(\tilde{\nu}, t)$ can be considered a time and wavenumber-dependent molar absorptivity. When these two are terms multiplied, the model function $Y(\tilde{\nu}, t)$ (3) resembles an analog to Beer's Law [83].

Fitting $Y(\tilde{\nu}, t)$ (3) to experimental data sets (e.g. Figure 4) will result in values for a number of model parameters (see section 3.2) which will reflect the chemical and physical information about the samples' adaptation processes.

3.2. Theory: Modeling Continually Changing Biomass

Once cells are in the range of the evanescent field, they are still growing. Therefore, any multiplication adds to the number of cells contributing to the observed signal increases. Cells of the species *Dunaliella salina* are around 10 µm in diameter [29] while the reach of the evanescent field is normally in the range of 0.5 to 2 µm [80]. For this reason, it was assumed that only the cells in the first layer of the biosediment can contribute to the spectroscopic signal. Once the ATR crystal is covered by the biosediment, spectroscopic signals will no longer increase. Thus, $A(t)$ represents the area of the ATR crystal covered by biomass at a given time while the total area of the crystal will be represented by $A_{\max} \geq A(t)$. Microalgae cells were also assumed to be distributed homogeneously within the growth medium which means that every point on the crystal is equally likely to have a cell deposit there. Therefore, the increase in covered area over time is proportional to the area that has not been covered, as described by $\frac{\mathrm{d}A}{\mathrm{d}t} \propto \left(A_{\max} - A(t)\right)$. By adding an

unknown, time dependent function $\varphi(t)$ the relationship becomes a first-order ordinary differential equation (ODE) [83]:

$$\frac{dA}{dt} = \varphi(t) \cdot \left(A_{max} - A(t)\right)$$

(4)

The function $\varphi(t)$ is made up of three parts. The higher the sinking velocity v_{sink} of the cells, the faster the biosediment is created. The size of the cell S_{cell} also contributes to the formation of biosediment. The larger the cell size, the more area of the ATR element that is covered by each cell depositing on the crystal. Lastly, the higher the density of the culture $\rho_{\mathrm{cell}}(t)$ the more cells that reach the bottom of the container and the faster the biosediment builds up. Putting these three terms together leads to the equation [83]:

$$\varphi(t) = S_{cell} \cdot v_{sink} \cdot \rho_{cell}(t)$$

(5)

The cell size depends on the species of algae and was considered to be constant. The sinking velocity depends on the net force experienced by the cells between gravity and buoyancy. Gravity and buoyancy were considered to be constant therefore v_{sink} was only determined by the amount of time the accelerating force was acting on the algae cells. For the purpose of this study, however, the acceleration was assumed to be so small that the sinking velocity was approximately constant. The viscosity and density of the growth medium were also assumed to be constant and were considered part of the sinking velocity. Suspended cells in the medium and in the biosediment still continue to grow and multiply. Therefore, the cell concentration $\rho_{\mathrm{cell}}(t)$ is therefore described by a sigmoidal function of time t [79]:

$$\rho_{cell}(t) = \rho_{max} \cdot \frac{1}{\left(1 + e^{\left(-\frac{\rho_{max}}{\rho_{max} - \rho_0} \cdot s \cdot (t - t_0)\right)} \cdot \left(\frac{\rho_{max}}{\rho_0} - 1\right)\right)}$$

(6)

In equation (6), $\rho_{\max}$ represents the maximum cell concentration that can be successfully supported in a given environment, ρ_0 expresses the initial cell concentration when the algal suspension is placed in the liquid ATR cell, and s, the cellular growth rate, represents the rate at which a culture's cellular density increases under a particular set of growth conditions. Inserting (5) and (6) into (4) leads to equation (7), an ODE that can be solved by the method of separation of variables [83], [85].

$$\frac{1}{A_{max}-A}dA = S_{cell}\cdot \nu_{sink}\cdot\ \rho_{max}\cdot \frac{1}{\left(1+e^{\left(-\frac{\rho_{max}}{\rho_{max}-\rho_0}\cdot s\cdot(t-t_0)\right)}\cdot\left(\frac{\rho_{max}}{\rho_0}-1\right)\right)}\cdot dt \qquad (7)$$

Solving for (7) results in (8) where C is an integration constant [83].

$$A(t) = A_{max} - C\cdot\left(1+\frac{\rho_{max}-\rho_0}{\rho_0}\cdot e^{\left(\frac{\rho_{max}}{\rho_{max}-\rho_0}\cdot s\cdot(t-t_0)\right)}\right)^{-S_{cell}\cdot\nu_{sink}\cdot\frac{\rho_{max}-\rho_0}{s}} \qquad (8)$$

Equation (8) describes how the total area of the ATR crystal $A_{\max}$ is covered by microalgae cells. Model parameters that will be eventually determined via nonlinear least-squares regression were introduced into (8), resulting in (9) [83]:

$$A(t) = \theta_1 - \theta_2\cdot\left(1+\theta_3\cdot e^{(\theta_4\cdot(t-\theta_5))}\right)^{-\theta_6} \qquad (9)$$

Although equation (9) describes the formation of biosediment, it does not account for any chemistry that occurs in the microalgae cells for the duration of the analysis. The chemically changing biomass leads to the production of time-dependent spectroscopic signal, denoted as $\varepsilon(\tilde{\nu},t)$ in (3). This function is comprised of four complementary contributions to the absorbance: a term describing the expenditure of reactants, the formation and consumption of any intermediates, the creation of products, and one static term. These terms can be combined and expressed as $\varepsilon(\tilde{\nu},t) = \varepsilon_{\text{static}}(\tilde{\nu}) +$

$\varepsilon_{\text{reactant}}(\tilde{\nu},t)+\varepsilon_{\text{intermediate}}(\tilde{\nu},t)+\varepsilon_{\text{product}}(\tilde{\nu},t)$ [83]. Any information gained about the molar absorptivities within these terms can reveal what compounds are contained within the sample at a given point in time. The time scale on which changes happen then reveal the dynamics of the microalgae's chemical adaptations.

Since both the reaction order of these processes and the number of reactions at a distinct wavenumber are unknown, the modelling of this system had to be simplified by making two assumptions. First, it was assumed that only one analyte absorbed at a given wavenumber although different analytes could absorb at different wavenumbers. The second assumption was that chemical processes occurring within the microalgae took place as two successive first-order reactions i.e. $A \overset{k_1}{\rightarrow} B \overset{k_2}{\rightarrow} C$. Thus, the time-dependent concentrations of reactant A, intermediate B, and product C, can be expressed as [86]:

$$[A]_t = [A]_0 \cdot e^{-k_1 \cdot t}$$

$$[B]_t = [A]_0 \cdot \frac{k_1}{k_2 - k_1} \cdot (e^{-k_1 \cdot t} - e^{-k_2 \cdot t})$$

$$[C]_t = [A]_0 \cdot \left(1 - \frac{k_2}{k_2 - k_1} \cdot e^{-k_1 \cdot t} + \frac{k_1}{k_2 - k_1} \cdot e^{-k_2 \cdot t}\right)$$

(10)

The time-dependent concentrations were multiplied by unknown molar absorptivities, $a(\tilde{\nu})$, of the reactant, intermediate, and product, respectively. This led to equations (11) - (13) [83].

$$\varepsilon_{reactant}(\tilde{\nu},t) = a_{reactant}(\tilde{\nu}) \cdot [A]_t = a_{reactant}(\tilde{\nu}) \cdot [A]_0 \cdot e^{-k_1 \cdot t}$$

(11)

$$\begin{aligned}\varepsilon_{intermediate}(\tilde{\nu},t) &= a_{intermediate}(\tilde{\nu}) \cdot [B]_t \\ &= a_{intermediate}(\tilde{\nu}) \cdot [A]_0 \cdot \frac{k_1}{k_2 - k_1} \cdot (e^{-k_1 \cdot t} - e^{-k_2 \cdot t})\end{aligned}$$

(12)

$$\begin{aligned}\varepsilon_{product}(\tilde{\nu},t) &= a_{product}(\tilde{\nu}) \cdot [C]_t \\ &= a_{product}(\tilde{\nu}) \cdot [A]_0 \cdot \left(1 - \frac{k_2}{k_2 - k_1} \cdot e^{-k_1 \cdot t} + \frac{k_1}{k_2 - k_1} \cdot e^{-k_2 \cdot t}\right)\end{aligned}$$

(13)

In (11), $a_{\text{reactant}}(\tilde{\nu}) \cdot [A]_0$ was replaced with $\theta_8(\tilde{\nu})$ and k_1 was replaced with $\theta_9(\tilde{\nu})$, leading to equation (14). Within (12), $a_{\text{intermediate}}(\tilde{\nu}) \cdot [A]_0 \cdot \frac{k_1}{k_2 - k_1}$ became $\theta_{10}(\tilde{\nu})$, k_1 became $\theta_{11}(\tilde{\nu})$, and k_2 became $\theta_{12}(\tilde{\nu})$, producing equation (15). Equation (13) featured the addition of five parameters; $a_{\text{product}}(\tilde{\nu}) \cdot [A]_0$ was replaced with $\theta_{13}(\tilde{\nu})$, the terms $\frac{k_2}{k_2 - k_1}$ and $\frac{k_1}{k_2 - k_1}$ became $\theta_{14}(\tilde{\nu})$ and $\theta_{16}(\tilde{\nu})$, respectively, and k_1 and k_2 were substituted with $\theta_{15}(\tilde{\nu})$ and $\theta_{17}(\tilde{\nu})$, respectively, to produce (16) [83].

$$\varepsilon_{reactant}(\tilde{\nu}, t) = \theta_8(\tilde{\nu}) \cdot e^{-\theta_9(\tilde{\nu}) \cdot t}$$

(14)

$$\varepsilon_{intermediate}(\tilde{\nu}, t) = \theta_{10}(\tilde{\nu}) \cdot \left(e^{-\theta_{11}(\tilde{\nu}) \cdot t} - e^{-\theta_{12}(\tilde{\nu}) \cdot t}\right)$$

(15)

$$\varepsilon_{product}(\tilde{\nu}, t) = \theta_{13}(\tilde{\nu}) \cdot \left(1 - \theta_{14}(\tilde{\nu}) \cdot e^{-\theta_{15}(\tilde{\nu}) \cdot t} + \theta_{16}(\tilde{\nu}) \cdot e^{-\theta_{17}(\tilde{\nu}) \cdot t}\right)$$

(16)

The parameters introduced into equations (11) - (13), however, differ from those in (9) as they are wavelength dependent and thus expressed as $\theta_i(\tilde{\nu})$. Furthermore, there may be compounds present in the biomass that do not undergo reaction. These compounds add a time-independent but wavenumber-dependent contribution to the absorbance spectrum. These static compounds are described by (17) in which $a_{\text{static}}(\tilde{\nu})$ represents the molar absorptivity of these compounds and $[S]$ their concentrations. These two terms were then combined into $\theta_7(\tilde{\nu})$ [83].

$$\varepsilon_{static}(\tilde{\nu}) = a_{\text{static}}(\tilde{\nu}) \cdot [S] = \theta_7(\tilde{\nu})$$

(17)

Equations (14) - (17) were then combined into (18) which fully describes the time-dependent spectroscopic contributions of all chemical species [83].

$$\varepsilon(\tilde{\nu}, t) = \theta_7(\tilde{\nu}) + \theta_8(\tilde{\nu}) \cdot e^{-\theta_9(\tilde{\nu}) \cdot t} + \theta_{10}(\tilde{\nu}) \cdot \left(e^{-\theta_{11}(\tilde{\nu}) \cdot t} - e^{-\theta_{12}(\tilde{\nu}) \cdot t}\right) + \theta_{13}(\tilde{\nu}) \cdot \left(1 - \theta_{14}(\tilde{\nu}) \cdot e^{-\theta_{15}(\tilde{\nu}) \cdot t} + \theta_{16}(\tilde{\nu}) \cdot e^{-\theta_{17}(\tilde{\nu}) \cdot t}\right)$$

(18)

The last parameter added to the model function $Y(\tilde{\nu},t)$ is a term that accounts for any spectroscopic baseline drift, designated as $\theta_{18}(\tilde{\nu})$. Therefore, the final model function that spectroscopic time series will be fitted to is described by (19) [83]. All parameters and their meanings are listed in Table 4.

$$\begin{aligned} Y(\tilde{\nu},t) &= A(t)\cdot\varepsilon(\tilde{\nu},t)+\theta_{18}(\tilde{\nu}) \\ &= \left[\theta_1-\theta_2\cdot\left(1+\theta_3\cdot e^{\left(\theta_4\cdot(t-\theta_5)\right)}\right)^{-\theta_6}\right] \\ &\cdot\left[\theta_7(\tilde{\nu})+\theta_8(\tilde{\nu})\cdot e^{-\theta_9(\tilde{\nu})\cdot t}+\theta_{10}(\tilde{\nu})\cdot\left(e^{-\theta_{11}(\tilde{\nu})\cdot t}-e^{-\theta_{12}(\tilde{\nu})\cdot t}\right)+\theta_{13}(\tilde{\nu})\right. \\ &\cdot\left.\left(1-\theta_{14}(\tilde{\nu})\cdot e^{-\theta_{15}(\tilde{\nu})\cdot t}+\theta_{16}(\tilde{\nu})\cdot e^{-\theta_{17}(\tilde{\nu})\cdot t}\right)\right]+\theta_{18}(\tilde{\nu}) \end{aligned} \quad (19)$$

By using nonlinear least-squares regression of experimental data to solve for the parameters in the model function (19), chemical and physical properties of the microalgae system were deduced. By comparing the parameter values obtained from the benchmark spectroscopic series to the values from the series with an increase in carbon dioxide concentration, information regarding microalgae's adaptation processes in response to chemical shifts in their environment can be gained.

Table 4. List of all model parameters and their definitions [83].

Parameter	Definition
θ_1	A_{max}
θ_2	C (integration constant)
θ_3	$\frac{\rho_{max} - \rho_0}{\rho_0}$
θ_4	$\frac{\rho_{max}}{\rho_{max} - \rho_0} \cdot s$
θ_5	t_0
θ_6	$-S_{cell} \cdot \nu_{sink} \cdot \frac{\rho_{max} - \rho_0}{s}$
$\theta_7(\tilde{\nu})$	$a_{\text{static}}(\tilde{\nu}) \cdot [S]$
$\theta_8(\tilde{\nu})$	$a_{reactant}(\tilde{\nu}) \cdot [A]_0$
$\theta_9(\tilde{\nu})$	k_1
$\theta_{10}(\tilde{\nu})$	$a_{\text{intermediate}}(\tilde{\nu}) \cdot [A]_0 \cdot \frac{k_1}{k_2 - k_1}$
$\theta_{11}(\tilde{\nu})$	k_1
$\theta_{12}(\tilde{\nu})$	k_2
$\theta_{13}(\tilde{\nu})$	$a_{\text{product}}(\tilde{\nu}) \cdot [A]_0$
$\theta_{14}(\tilde{\nu})$	$\frac{k_2}{k_2 - k_1}$
$\theta_{15}(\tilde{\nu})$	k_1
$\theta_{16}(\tilde{\nu})$	$\frac{k_1}{k_2 - k_1}$
$\theta_{17}(\tilde{\nu})$	k_2
$\theta_{18}(\tilde{\nu})$	Spectroscopic offset

3.3. Nonlinear Least-Squares Regression of Time-Dependent Spectroscopic Signatures

The final model function (19) contains multiple nonlinear model parameters. This often leads to the nonlinear fitting algorithm generating poor fit results due to multiple local minima present in the sum-of-squared errors (SSEs). Different starting points for the nonlinear regression can even cause different solutions to be produced [87]. There are multiple software packages that can perform nonlinear least-squares analysis [88] - [90], but the best way to avoid local minima is to provide the software with some initial prediction of acceptable values of model parameters. For this reason, a technique designated as Guided Random Search (GRS) [87] was employed. This approach first randomly explores the SSE hypersurface to predict probability density functions (pdfs) which express the possibility that a particular model parameter θ will lead to a low SSE with a high correlation coefficient. These pdfs are then used to lead a second, high-resolution exploration of the SSE hypersurface that concentrates on the model parameter ranges with the highest probability of producing a low SSE. The best set of model parameters found in this second examination of the hypersurface is then used as the initial estimates for the final nonlinear regression [83].

Before applying the GRS method, however, initial parameter ranges were selected. Since the parameters contain information about known chemical and physical properties, acceptable ranges can be determined which will further aid in avoiding local minima and producing a low SSE. To set boundaries for the formation of biosediment a range of 0 to 1 was selected for $\theta_{1,2,4}$, 0 to 1000 for θ_3, -500 to 500 for θ_5, and 0 to 0.2 for θ_6. The confines for θ_7 are dependent on whether or not negative absorbances were caused by baseline drift. If negative absorbances were caused by baseline drift, the relation $0 \leq \theta_7 \leq \Delta y(\tilde{\nu}, t) = \max(y_{n=1,\dots,N}) - \min(y_n)$ was chosen, where y_n represents measured data points. When negative absorbance does not occur, the inequality $0 \leq \theta_7 \leq \max(y_n)$ was used instead, which also leads to $\min(\theta_7) \leq \theta_{8,13} \leq \max(\theta_7)$. If no reactions take place then $\theta_{8,10,13}$ are assumed to be zero. Because of the time scale of the experiment, $\theta_{9,12,12,15,17}$ was given a range from 0 to 0.1 to resemble acceptable rate constants. Since

$k_2 - k_1$can be negative, values for $\theta_{10,14,16}$ could be negative or positive and the range of -100 to 100 was used. The last two situations are related to the spectroscopic baseline term θ_{18}. If a negative absorbance $y_0 < 0$ was observed at $t = 0$, a baseline drift has definitely occurred and thus requires consideration in the model. For this purpose, the following boundaries were chosen: $1.1 \cdot y_0 \leq \theta_{18} \leq 0.9 \cdot y_0$. If there is no negative absorbance at $t = 0$, baseline drift cannot be discriminated from a real spectroscopic signal and θ_{18} was set to 0 [83].

To further reduce the likelihood that the nonlinear least-squares regression ran into local minima, regression constraints were also added. Comparing the equations of the model functions, more information about the experimental environment can be included through the use of equality and inequality constraints [90], [91]. Five equality constraints were deduced from equation (19):

$$\theta_9(\tilde{\nu}) = \theta_{11}(\tilde{\nu}) = \theta_{15}(\tilde{\nu})$$

$$\theta_{12}(\tilde{\nu}) = \theta_{17}(\tilde{\nu})$$

$$\theta_{14}(\tilde{\nu}) = \frac{\theta_{12}(\tilde{\nu})}{\theta_{12}(\tilde{\nu}) - \theta_9(\tilde{\nu})}$$

$$\theta_{16}(\tilde{\nu}) = \frac{\theta_9(\tilde{\nu})}{\theta_{12}(\tilde{\nu}) - \theta_9(\tilde{\nu})}$$

(20)

Four inequality constraints were also extracted from the model function. The area of the ATR crystal coated with microalgae at time t cannot have a negative value, therefore, $\theta_1 \geq \theta_2 \cdot \left(1 + \theta_3 \cdot e^{(\theta_4 \cdot (t - \theta_5))}\right)^{\theta_6}$. Intermediates are formed and then consumed during the reaction process and theoretically should have a peak of spectroscopic contribution so any spectroscopic signal created by these species cannot be less than zero. This leads to the inequality constraint $\theta_{10}(\tilde{\nu}) \cdot \left(e^{-\theta_{11}(\tilde{\nu}) \cdot t} - e^{-\theta_{12}(\tilde{\nu}) \cdot t}\right) \geq 0$. Similarly, the spectroscopic signal originating from product will be non-negative, which leads to the inequality constraint: $\theta_{13}(\tilde{\nu}) \cdot \left(1 - \theta_{14}(\tilde{\nu}) \cdot e^{-\theta_{15}(\tilde{\nu}) \cdot t} + \theta_{16}(\tilde{\nu}) \cdot e^{-\theta_{17}(\tilde{\nu}) \cdot t}\right) \geq 0$. By making the assumption that reactions in the algal system proceeded as two consecutive first-

order reactions, once product is formed, it cannot be removed, and as such its contribution cannot decrease. Thus, the last inequality constraint is: $\frac{d}{dt}\left[\theta_{13}(\tilde{\nu}) \cdot \left(1 - \theta_{14}(\tilde{\nu}) \cdot e^{-\theta_{15}(\tilde{\nu}) \cdot t} + \theta_{16}(\tilde{\nu}) \cdot e^{-\theta_{17}(\tilde{\nu}) \cdot t}\right)\right] = \theta_{13}(\tilde{\nu}) \cdot \theta_{14}(\tilde{\nu}) \cdot \theta_{15}(\tilde{\nu}) \cdot e^{-\theta_{15}(\tilde{\nu}) \cdot t} - \theta_{13}(\tilde{\nu}) \cdot \theta_{16}(\tilde{\nu}) \cdot \theta_{17}(\tilde{\nu}) \cdot e^{-\theta_{17}(\tilde{\nu}) \cdot t} \geq 0$ [83].

Furthermore, nonlinear regression of this system can be approached in two ways. First, SSE is minimized by incorporating all n wavenumber positions into one regression. Since $A(t)$ is not wavenumber dependent, this is desirable as it ensures the values for $\theta_{1\ldots6}$ are consistent for all wavenumbers. This approach leads to a large number of model parameters, i.e. $6 + N \cdot 12 = 6 + 208 \cdot 12 = 2502$, which could cause a higher chance of the algorithm getting trapped in a local minima. The second approach was to model $n = 208$ wavenumbers independently, which only involves eighteen model parameters each, thus greatly reducing the chance of running into a local minima for each fit [83].

A final assumption made for this model is that any reaction taking place only occurred at one wavenumber, i.e. reactant, product, and intermediate all absorbed at the same wavenumber. This assumption allowed the molar absorptivities, such as $a_{reactant}(\tilde{\nu})$ in $\theta_8(\tilde{\nu})$ (11), (14), to remain constant for each chemical species, which meant that any change in model parameters $\theta_{7,8,10,13}(\tilde{\nu})$ were due to changes in concentrations of these compounds.

3.4. Conclusions

Changes in observed spectroscopic signal over time are due to two processes that occur in microalgae during the twelve hour analysis period. These two processes include the formation of biosediment on the ATR element and any chemical reactions that take place within the microalgae. The formation of biosediment is dependent on multiple factors, such as the cultures' cellular density, the growth rate of the culture, the buoyancy of the cells in the sample, but is wavenumber independent. All these factors were incorporated into (8) and simplified through the use of model parameters into (9). The chemical

contribution to spectroscopic signals is due to the loss of reactant, the rise and fall of intermediate compounds, the creation of product, and any chemical compounds that do not undergo a chemical reaction. These four factors were described with equations (14) - (17), respectively and were added, along with (9) and a spectroscopic offset term, to form the final model equation described by (19). This model function was then used to carry out a nonlinear least-squares regression of experimental data sets. GRS helped to set boundaries for model parameters to aid in avoiding local minima and thus poor fits. As the model functions describe physical and chemical properties of the algal system, acceptable starting ranges for GRS were also determined. Finally, the comparison of all portions of the model function led to equality and inequality constraints to further decrease the chances of running into local minima.

4. Results and Discussion

4.1. Introduction

The aim of this study was to model chemical changes algae underwent due to changing nutrient availability in their environment; of particular interest is bicarbonate, which originates from atmospheric carbon dioxide. The amount of bicarbonate dissolved in the cells' growing environment increases as the concentration of carbon dioxide in the atmosphere increases. Predictions about the impact of increased bicarbonate concentration on microalgal biomass were based on differences of spectroscopic time series collected at standard and elevated carbon dioxide concentration. Visual differences in the experimental data yield a qualitative assessment into changes the algae underwent. A comparison of the calculated model parameters in (19) offers a quantitative assessment of changes as each model parameter reflects a specific chemical or physical property of the algal biomass.

4.2. Individual Wavenumber Modeling of Spectroscopic Time Series

The model function $Y(\tilde{\nu}, t)$ (19) was fitted wavenumber-by-wavenumber to collected spectroscopic time series, in 10 cm^{-1} intervals, through the selected 1350 - 950 cm^{-1} range; $Y(\tilde{\nu}, t)$ was fitted to three spectroscopic time series at each bicarbonate concentration. Figure 5 depicts an experimental spectroscopic time series at standard carbon dioxide concentration and the model obtained from its nonlinear fitting. As described in (19), the model obtained for each wavenumber is comprised of the biosediment formation, spectroscopic signal of chemical species, and a spectroscopic offset. The final model function was generated by multiplying the total spectroscopic contribution of chemical species (18) (Figure 6, top) by the formation of biosediment (8) (Figure 6, bottom) and adding the spectroscopic offset term (not pictured). The blue curve in Figure 7 represents the model function that is a result of this operation.

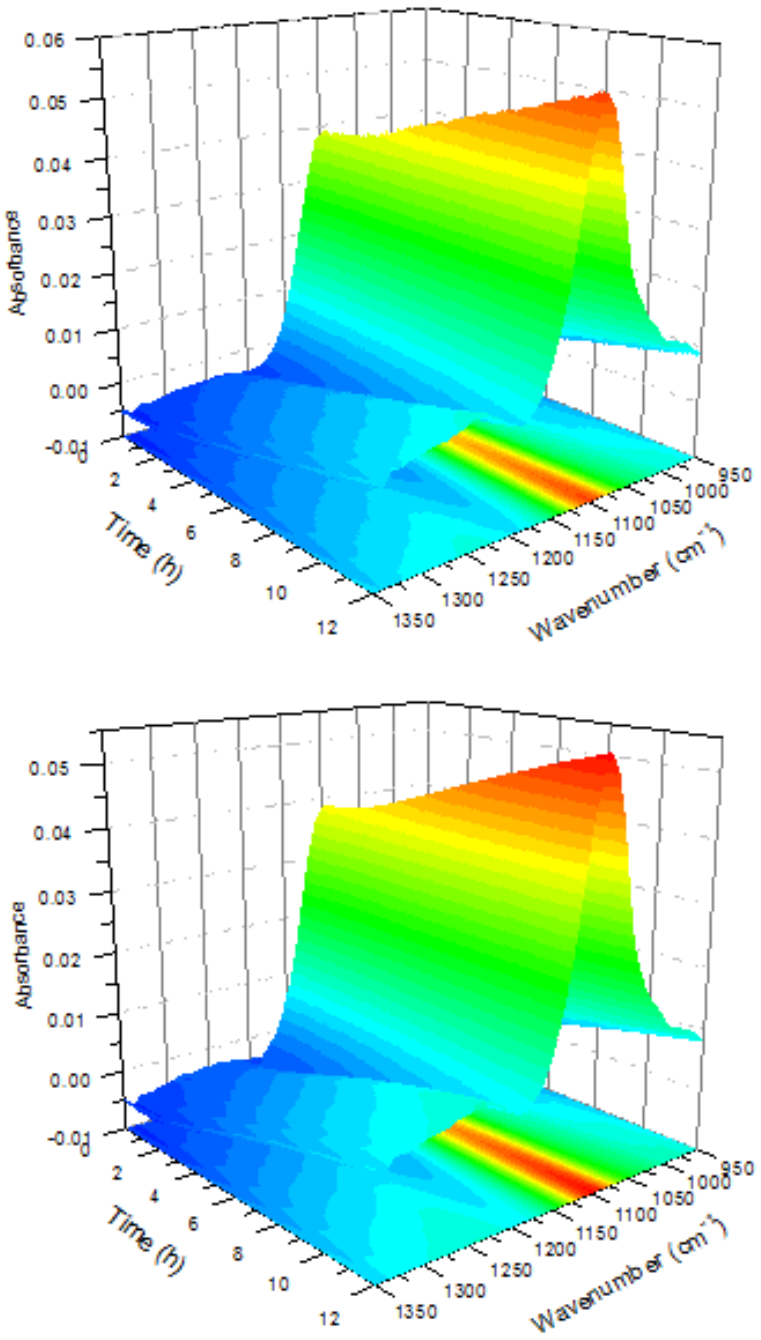

Figure 5. A comparison of the first twelve hours of a typical spectroscopic time series (top) and the model (bottom) of such a series obtained from nonlinear least-squares regression. Since the fitting was performed on a wavenumber-by-wavenumber basis, results had to be compiled into one dataset to produce the graph of the model in the bottom image.

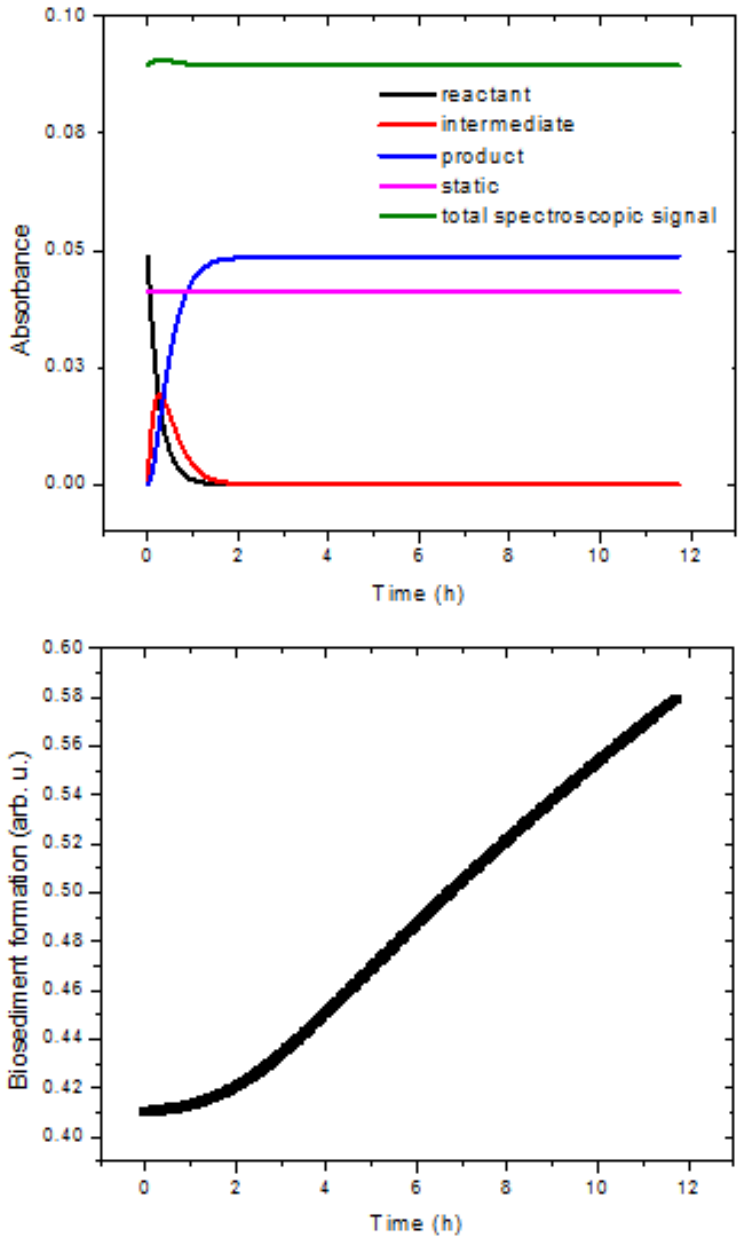

Figure 6. Spectroscopic contribution of all chemical species $\varepsilon(\tilde{\nu}, t)$ (18) (top) and formation of biosediment $A(t)$ (8) (bottom) at 1100 cm^{-1} for algae sample at standard bicarbonate concentration.

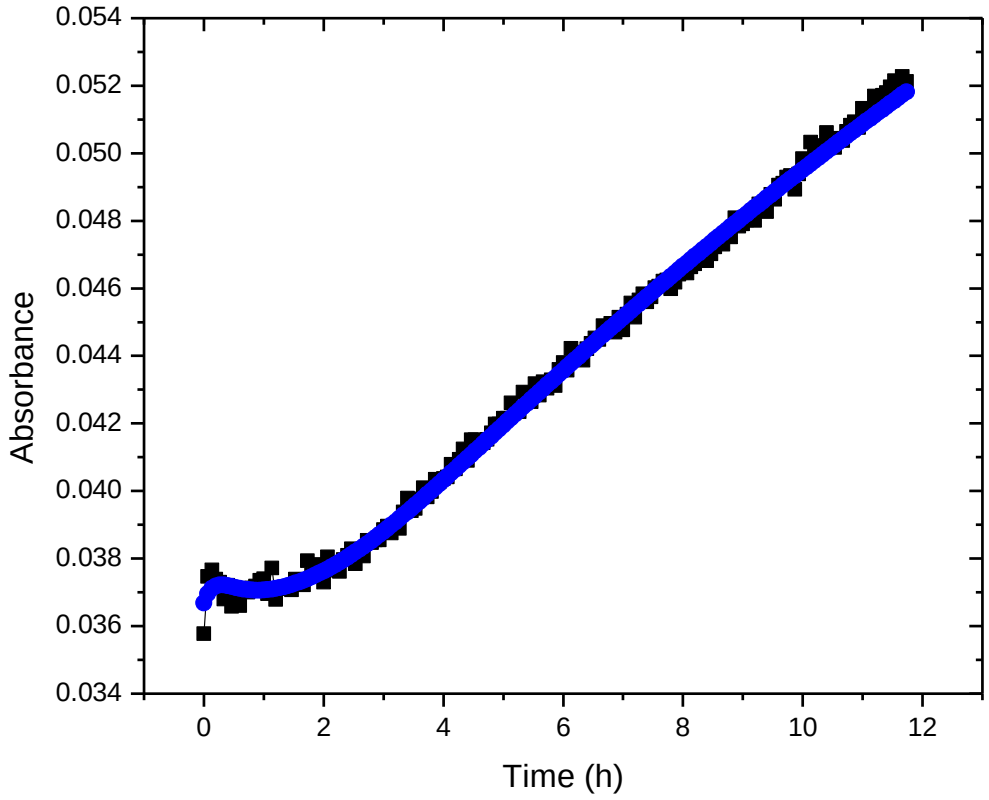

Figure 7. Obtained experimental spectroscopic time series (■) at 1100 cm^{-1} with its fitted model function (●) of sample at standard bicarbonate concentration.

For an initial examination into how the model and its components changed from standard to elevated bicarbonate concentration, the model components of two bands were closely examined: 1100 cm^{-1} and 1230 cm^{-1}. The band at 1100 cm^{-1} was chosen because of the large peak that was featured there in elevated bicarbonate samples (Figure 5). This band is also relevant because it may originate from polysaccharides, which have a high biological relevance in microalgal biomass [67], [92]. The 1230 cm^{-1} band was another band that increased over the duration of the experiment; this band is also relevant as it may arise from the presence of proteins or nucleic acids [67], [92].

Averages of model components at each bicarbonate level were compared to reach a better understanding of possible differences in these two bands caused by increased bicarbonate; four comparisons at 1100 cm^{-1} are pictured in Figure 8 and four comparisons at 1230 cm^{-1} are pictured in Figure 9. At 1100 cm^{-1}, the initial spectroscopic signal due to reactant decreased from standard to elevated bicarbonate concentration and the rate at which the absorbance decreased was slower in the elevated bicarbonate samples (Figure 8A). In Figure 8B, spectroscopic contribution of intermediates reaches a higher peak but the decrease of signal from this peak occurs at a slower rate in the elevated bicarbonate samples. Spectroscopic signal of product in standard bicarbonate samples reaches a higher level than that of the elevated bicarbonate samples, which is pictured in Figure 8C. Though it is not pictured, the contribution of static compounds was greater in samples of standard bicarbonate concentration. In Figure 8D, the biosediment coverage in the standard bicarbonate samples was greater for the entire time period but the rate at which the biosediment formed was greater in the elevated bicarbonate samples.

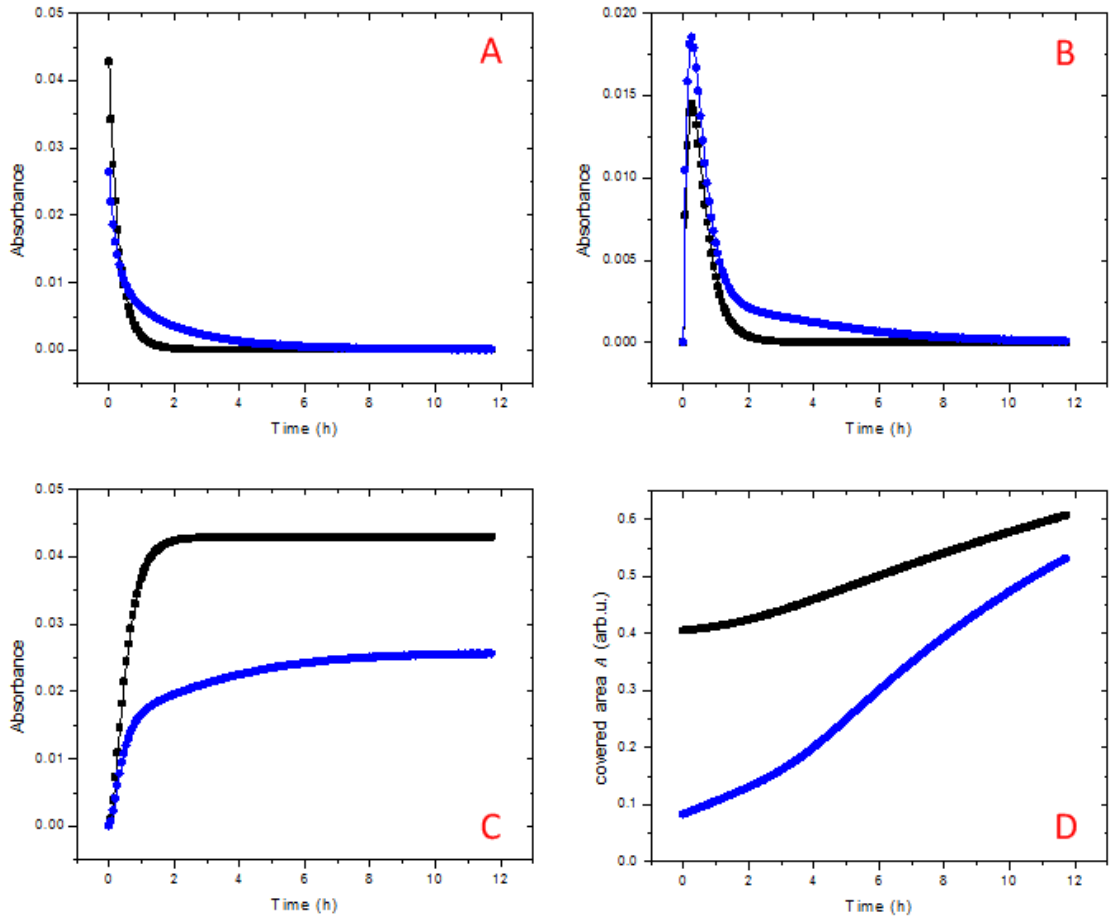

Figure 8. Comparison of spectroscopic contribution of four model components, reactants (A), intermediates (B), products (C), and biofilm formation (D), at standard (■) and elevated (●) bicarbonate concentration for the 1100 cm^{-1} band.

The comparison presented in Figure 9 appears to be different than that of 1100 cm^{-1}. Unlike the spectroscopic contribution of reactants at 1100 cm^{-1}, Figure 9A shows that the initial concentration of reactants is higher in elevated bicarbonate samples but still seems to decrease at a slower rate than the standard bicarbonate samples. In Figure 9B the contributions of intermediate species at both bicarbonate levels reached about the same level at their peak and the elevated bicarbonate sample again appeared to decrease at a slower rate. Again unlike 1100 cm^{-1}, the spectroscopic contribution of products (Figure 9C) increased in elevated bicarbonate samples. The intermediate contribution of elevated bicarbonate samples in Figure 9B did not return to 0 and the elevated bicarbonate samples' contribution of product did not plateau (Figure 9C), which implies the reaction at this wavenumber did not reach conclusion within twelve hours. The static compounds (not pictured) at this wavenumber were also different from 1100 cm^{-1} as the contribution was higher in the elevated bicarbonate samples. The biosediment formation at 1230 cm^{-1} (Figure 9D) appeared to be more consistent between bicarbonate levels than the formation at 1100 cm^{-1}.

In an ideal steady-state environment in which spent nutrient is constantly replenished, it was predicted that no reaction would occur in the biomass and, therefore, the spectroscopic contribution of reactants should be approximately zero. This prediction was not found to be the case as spectroscopic contribution of reactant does exist in these samples. The behavior of reactant at the two featured wavenumbers in Figure 8 and 9 suggest that a shift in reaction occurred as spectroscopic contribution of reactant decreased at 1100 cm^{-1} and increased at 1230 cm^{-1} in the elevated bicarbonate samples. The results presented in Figure 8 and 9 suggest that increased bicarbonate concentration leads to altered rates of reaction at both wavenumbers and a shift from the reaction occurring at 1100 cm^{-1} to that of 1230 cm^{-1}. It is also important to note that Figure 8D and 9D should theoretically be identical, but the wavenumber-by-wavenumber approach causes discrepancies in values at different wavenumbers.

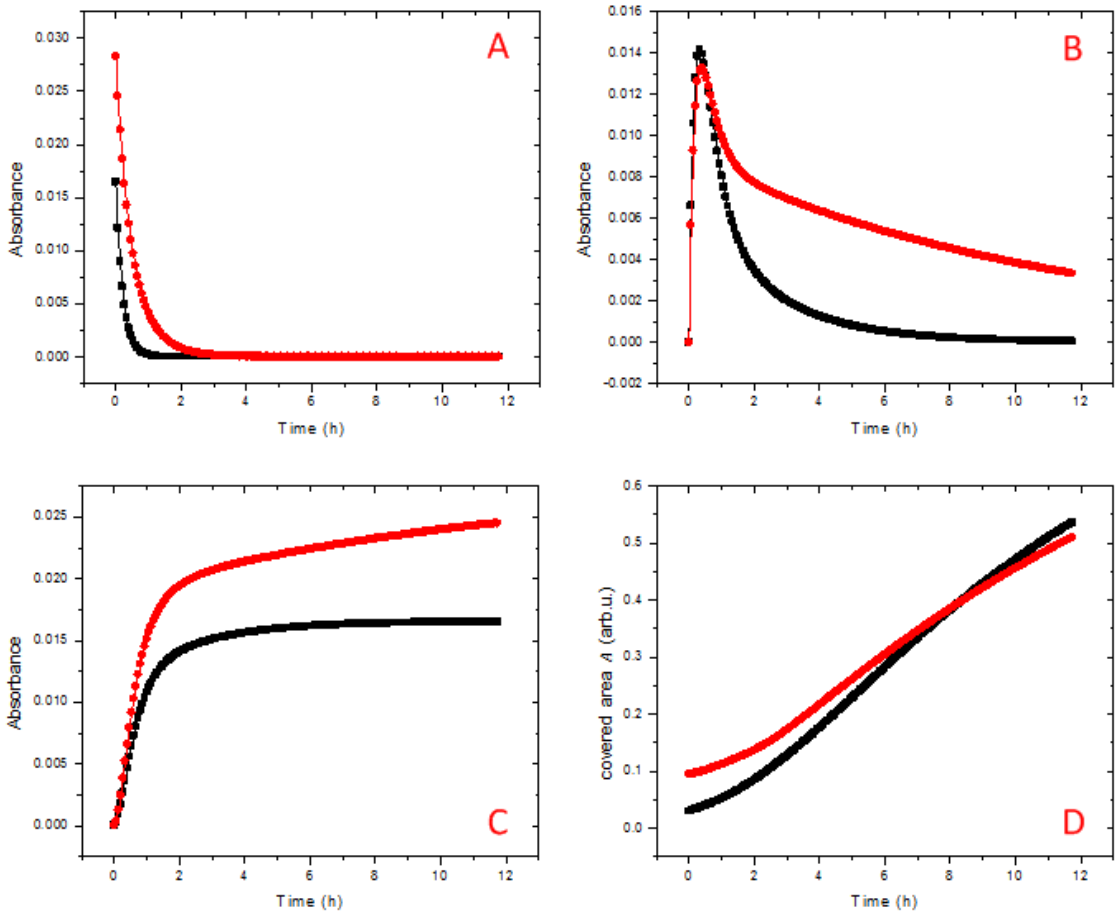

Figure 9. Comparison of spectroscopic contribution of four model components, reactants (A), intermediates (B), products (C), and biofilm formation (D), at standard (■) and elevated (●) bicarbonate concentration for the 1230 cm^{-1} band.

The examination of how model parameters (19) change from standard to elevated bicarbonate concentration can yield a more detailed perspective of the response of algae to elevated bicarbonate levels than a visual comparison of the model components. The model parameters $\theta_{1\ldots6}$ (9) are wavenumber independent because they are associated with physical cell characteristics and the formation of the biosediment.

Theoretically, the values obtained for these parameters should be the same at all wavelengths. However, because each wavenumber was fitted individually different sets of $\theta_{1\ldots6}$ were obtained for each wavenumber. Therefore, values for each parameter were averaged over all wavenumbers for the three replicates at standard conditions and the three replicates at elevated carbon conditions, (Figure 10). The three resulting values obtained from samples at each bicarbonate concentration were then averaged and analyzed for statistical differences using a t-test at a 95% confidence level.

The t-test showed that the averaged values for $\theta_{1,2,3,6}$ were not statistically different between the two bicarbonate concentrations and therefore do not appear to be affected by increased bicarbonate. It was expected that $\theta_1 = A_{max}$ (8) would be consistent at both levels of carbon dioxide as it simply corresponds to the area of the ATR crystal, which did not change between experiments. θ_3 (8), (9) is comprised of two terms: ρ_{max}, the maximum cell concentration that can be maintained at a particular culturing environment, and ρ_0, the cell concentration at $t = 0$. While it has been shown that ρ_{max} depends on the nutrient availability of the algae [79], [93], these studies were performed over multiple days; the twelve hour time span of the experiment may have not been enough to induce a significant change in ρ_{max}. The initial cell concentration ρ_0 was expected to be consistent from sample to sample because of how algae samples were prepared. For these reasons, the lack of change in θ_3 due to increased bicarbonate concentration is consistent with expectations. The parameter θ_6 also contains the terms ρ_{max} and ρ_0 along with two other terms, S_{cell} and v_{sink}. Even though S_{cell} has also been shown to be affected by nutrient availability in culture medium [26], [51] the relatively short time span of this experiment again likely limited possibilities to see significant change in this term. The buoyancy exerted on the cells presumably changed very little due to increased bicarbonate concentration, so v_{sink} should have been consistent

between the two bicarbonate levels. Therefore, since S_{cell} and ν_{sink} likely remained stable for the twelve hour analysis, the lack of significant change in θ_6 due to increased bicarbonate was reasonable. Model parameter θ_2 is an integration constant obtained when the ODE in (7) is solved. Since the derivation of θ_2 depends on terms that were expected to remain fairly consistent (A_{max}, ρ_{max}, ρ_0, S_{cell}, ν_{sink}) (7), (8), its lack of significant change is also reasonable.

The two parameters θ_4 and θ_5, on the other hand, were found to be significantly higher and lower, respectively, in the samples cultured with increased bicarbonate concentration. Because values of ρ_{max} are a few orders of magnitude greater than values of ρ_0 within model parameter θ_4 (8), (9), the value for $\frac{\rho_{max}}{\rho_{max}-\rho_0}$ can be assumed to be ≈ 1. Therefore, the increase in θ_4 was likely due to an increase in the rate at which the cellular concentration increases s. This result is also consistent with previous studies on how carbon dioxide affects cell growth and multiplication. For example, Azov demonstrated that two species of microalgae featured larger growth and carbon uptake rates when higher concentrations of carbon dioxide were provided in the growth medium [94]. $\theta_5 = t_0$ (8), (9) is the time at which cultures were initially inoculated. Any changes in this parameters are due solely to the way in which cultures were monitored and its significant decrease was likely not caused by the increased bicarbonate available to the samples.

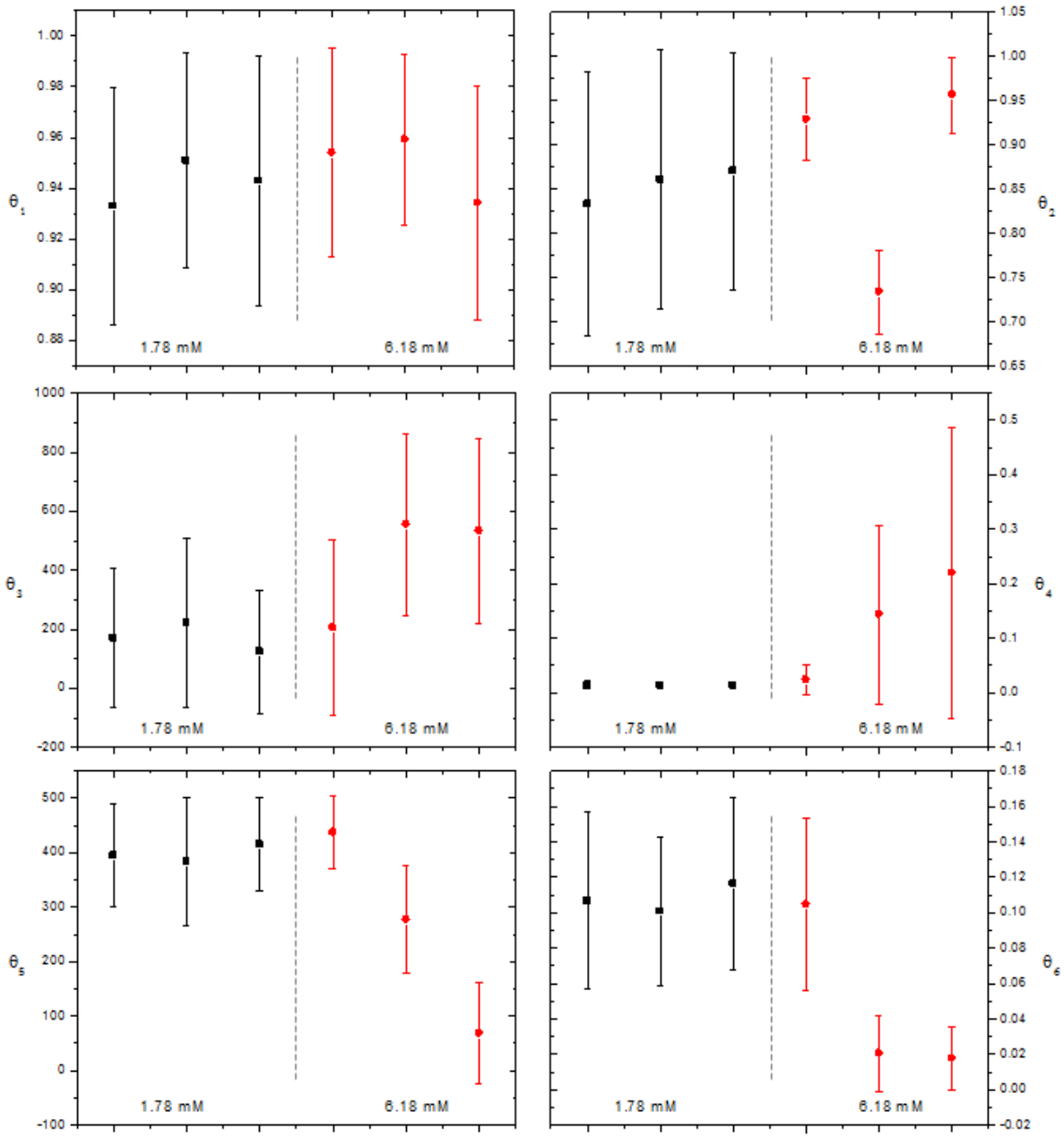

Figure 10. Averaged values of $\theta_{1\ldots6}$ obtained from nonlinear fitting of three replicate data sets each at standard (■) and elevated (●) bicarbonate concentrations.

Unlike $\theta_{1\ldots6}$, model parameters $\theta_{7\ldots17}$ represent chemical information such as the contributions of reactants, intermediates, and products to the spectroscopic signal as well as the rates at which these compounds are chemically changing. These parameters' values were averaged for the replicate cultures of both nutrient situations, followed by t-testing for significant changes between the two bicarbonate conditions (95% confidence interval). The results of t-tests for $\theta_{7,8,9,10,12,13}$ are depicted in Figure 14 - 16. If at a particular wavenumber position no significant difference between standard and elevated bicarbonate concentration was found, the t-test result has been indicated by a zero. If the value for the elevated bicarbonate environment is greater than the standard condition, the t-test result is expressed as a positive number; the opposite case has been indicated by a negative number. $\theta_{18}(\tilde{\nu})$ was not included in this discussion since it only accounts for spectroscopic baseline drifts.

Changes in the reaction rate constants $k_1 = \theta_9(\tilde{\nu})$ and $k_2 = \theta_{12}(\tilde{\nu})$ are presented in Figure 11 and 12, respectively. It is evident that results generated for these parameters did not change in response to increased concentration of bicarbonate. The differences in model components in the two nutrient conditions at 1100 cm^{-1} (Figure 8) and 1320 cm^{-1} (Figure 9) imply that the rate of reaction changed in elevated bicarbonate samples at these wavenumbers, but this is not reflected in the results for these rate constants. Even though each parameter had one wavenumber where a significant difference occurred, it is most likely that these significant differences were random and the model cannot resolve the rate of reactions taking place at any wavenumber.

In Figure 13 the differences in $\theta_{10}(\tilde{\nu})$, the spectroscopic contribution of intermediate compounds, are presented. Spectroscopic contribution of intermediate reached a higher peak (Figure 8) in samples with elevated bicarbonate samples so an increase in $\theta_{10}(\tilde{\nu})$ was expected at 1100 cm^{-1} due to elevated bicarbonate concentration. This was not found to be the case, however, as there was no significant change in $\theta_{10}(\tilde{\nu})$ between bicarbonate levels at any wavenumber and the values often featured large error bars; the model may have had difficulty in determining this term as well. The inconsistency of $\theta_{10}(\tilde{\nu})$ could also be due to it containing the term $\frac{k_1}{k_2 - k_1}$ (12), (15), which is comprised of two parameters that were already shown to be inconsistent (Figure 11 and 12).

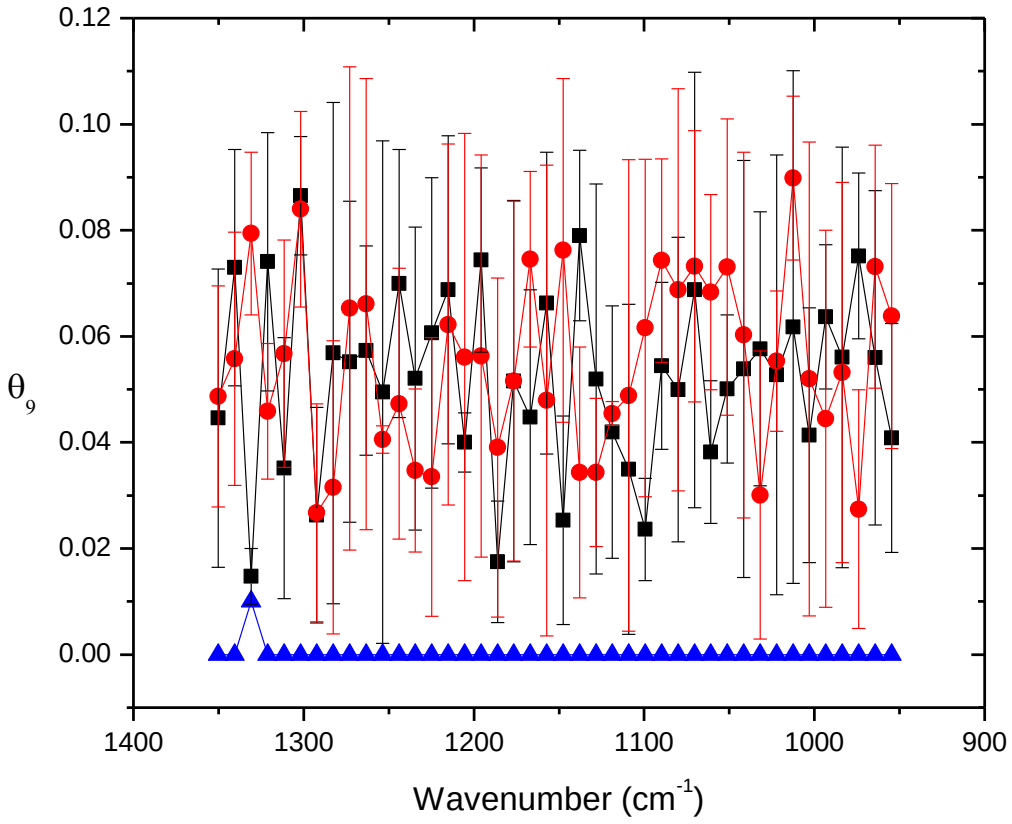

Figure 11. Effect of elevated bicarbonate levels on the model parameter $\theta_9(\tilde{\nu})$, the rate constant of step one of the two step first-order reaction. Positive t-test indicators (▲) depict wavenumbers at which the value for $\theta_9(\tilde{\nu})$ in the elevated bicarbonate sample (●) was significantly higher than the standard bicarbonate (■); a negative value indicates $\theta_9(\tilde{\nu})$ that is significantly lower.

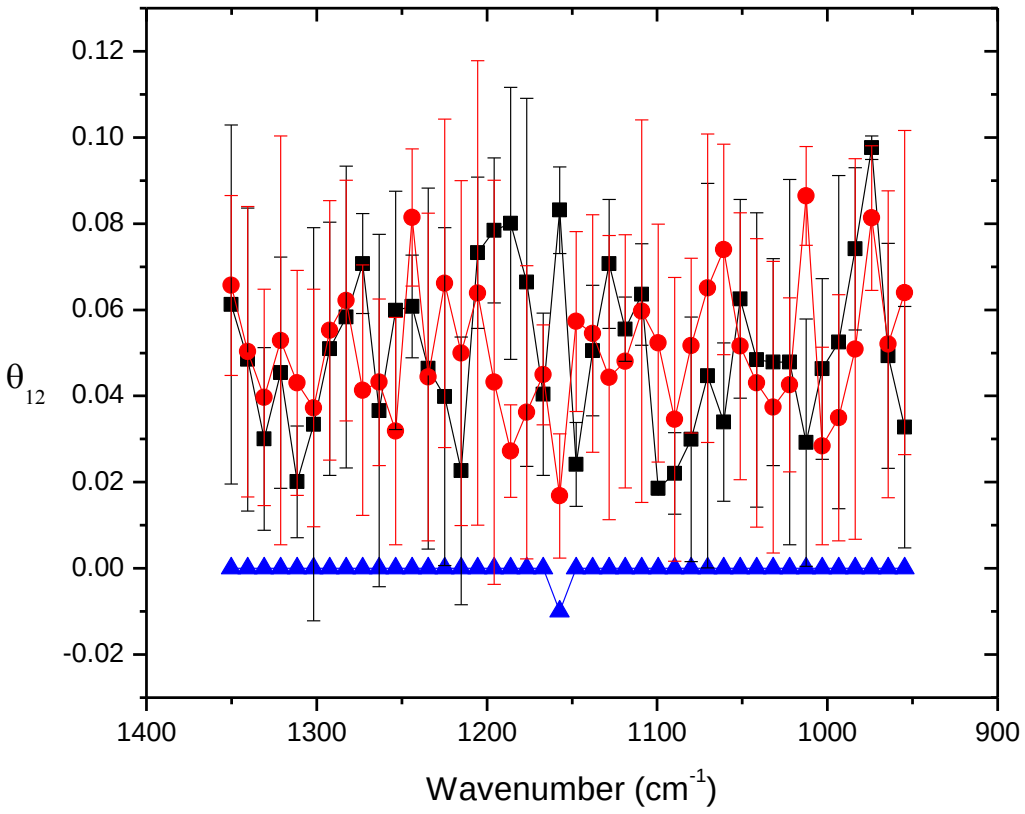

Figure 12. Effect of elevated bicarbonate levels on the model parameter $\theta_{12}(\tilde{\nu})$, the rate constant of step two of the two step first-order reaction. Positive t-test indicators (▲) depict wavenumbers at which the value for $\theta_{12}(\tilde{\nu})$ in the elevated bicarbonate sample (●) was significantly higher than the standard bicarbonate (■); a negative value indicates $\theta_{12}(\tilde{\nu})$ that is significantly lower.

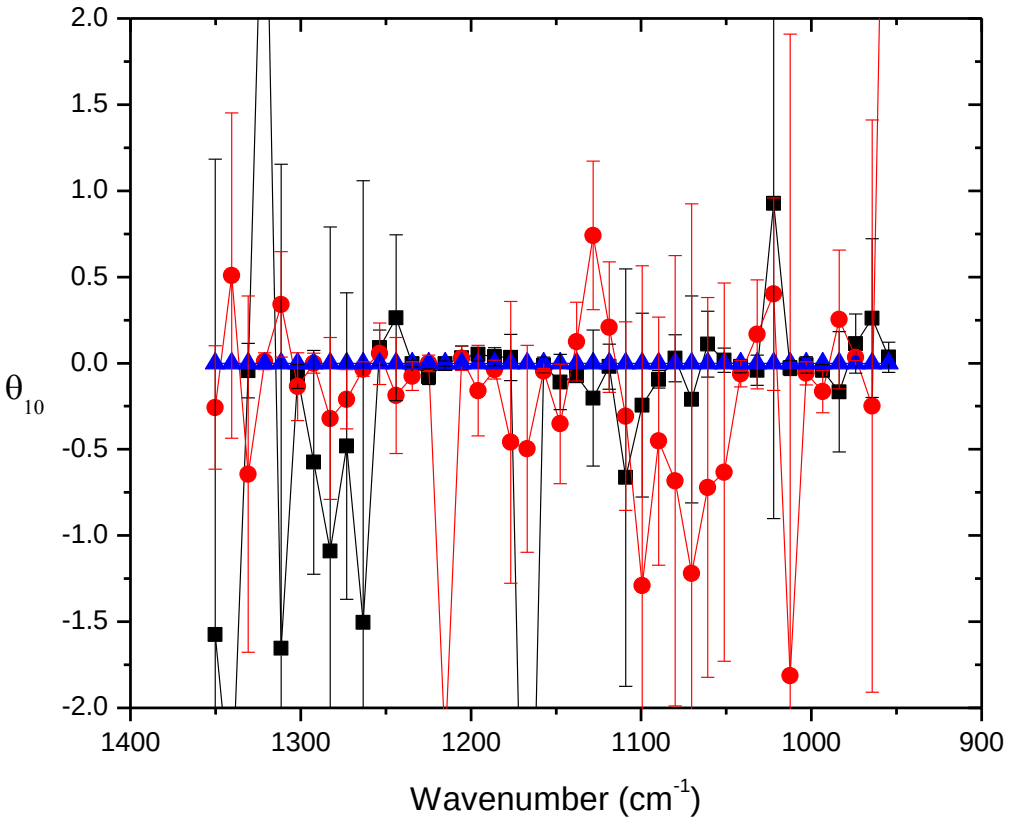

Figure 13. Effect of elevated bicarbonate levels on the model parameter $\theta_{10}(\tilde{\nu})$, the spectroscopic contribution of intermediate species in algal biomass. Positive t-test indicators (▲) depict wavenumbers at which the value for $\theta_{10}(\tilde{\nu})$ in the elevated bicarbonate sample (●) was significantly higher than the standard bicarbonate (■); a negative value indicates $\theta_{10}(\tilde{\nu})$ that is significantly lower.

The results of t-test analysis for model parameters $\theta_{7,8,13}(\tilde{\nu})$ all featured significant differences in their values at similar wavenumber positions. $\theta_7(\tilde{\nu})$, the spectroscopic contribution of static compounds (Figure 14), $\theta_8(\tilde{\nu})$, the spectroscopic contribution of reactant (Figure 15), and $\theta_{13}(\tilde{\nu})$, the spectroscopic contribution of product (Figure 16), all showed significant decreases at and around 1100 cm^{-1} and significant increases at multiple other wavenumbers outside of this band, including the 1320 cm^{-1} band. Many of the bands, including 1320 cm^{-1}, at which significant increases occurred could originate from proteins or nucleic acids. These results, along with the results presented in Figure 8 and 9, suggest that the increased concentration of bicarbonate caused a shift from production of polysaccharides towards production of proteins and nucleic acids. It has been shown that increased inorganic carbon in growth medium caused growth rates of algae to rise [94] and it is likely the significant increase in θ_4 was caused by a higher growth rate in elevated bicarbonate samples. The faster growth rate of the elevated bicarbonate samples could have caused energy stores in the form of polysaccharides to be used up for increased cellular division, thus causing greater presence of proteins and nucleic acids. Giordano and Bowes [51] observed that *D. salina* cells cultured with high carbon dioxide, and thus high bicarbonate, had higher growth rates and more protein content than those cultured with carbon dioxide levels the same as those present in the atmosphere, which further supports the explanation of the results for $\theta_{7,8,13}(\tilde{\nu})$.

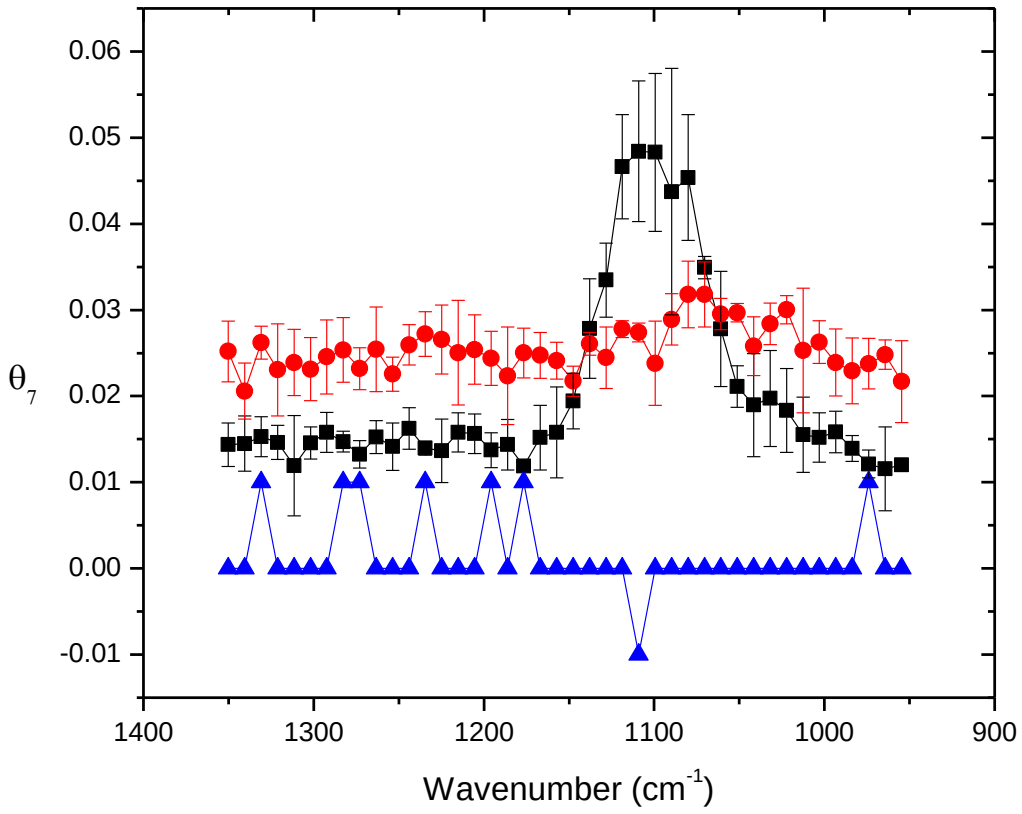

Figure 14. Effect of elevated bicarbonate levels on the model parameter $\theta_7(\tilde{\nu})$, the spectroscopic signal contribution from chemical compounds that do not participate in reactions. Positive t-test indicators (▲) depict wavenumbers at which the value for $\theta_7(\tilde{\nu})$ in the elevated bicarbonate sample (●) was significantly higher than the standard bicarbonate (■); a negative value indicates $\theta_7(\tilde{\nu})$ that is significantly lower.

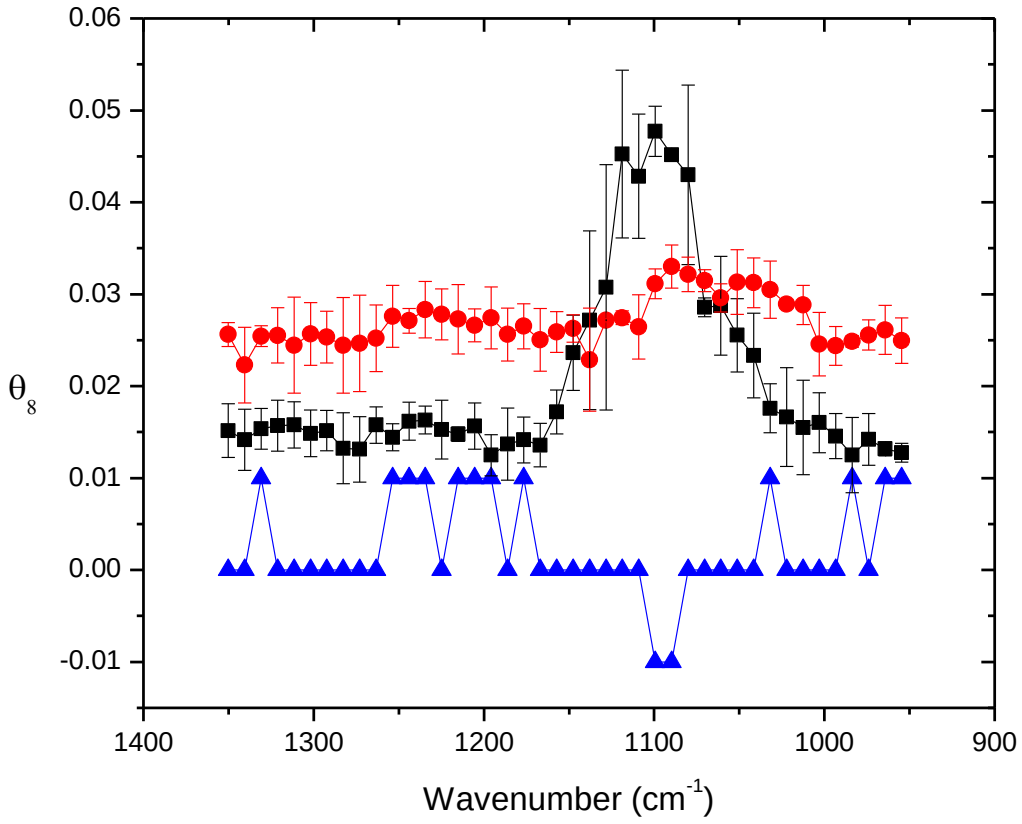

Figure 15. Effect of elevated bicarbonate levels on the model parameter $\theta_8(\tilde{\nu})$, the spectroscopic signal contribution of reactants in algal biomass. Positive t-test indicators (▲) depict wavenumbers at which the value for $\theta_8(\tilde{\nu})$ in the elevated bicarbonate sample (●) was significantly higher than the standard bicarbonate (■); a negative value indicates $\theta_8(\tilde{\nu})$ that is significantly lower.

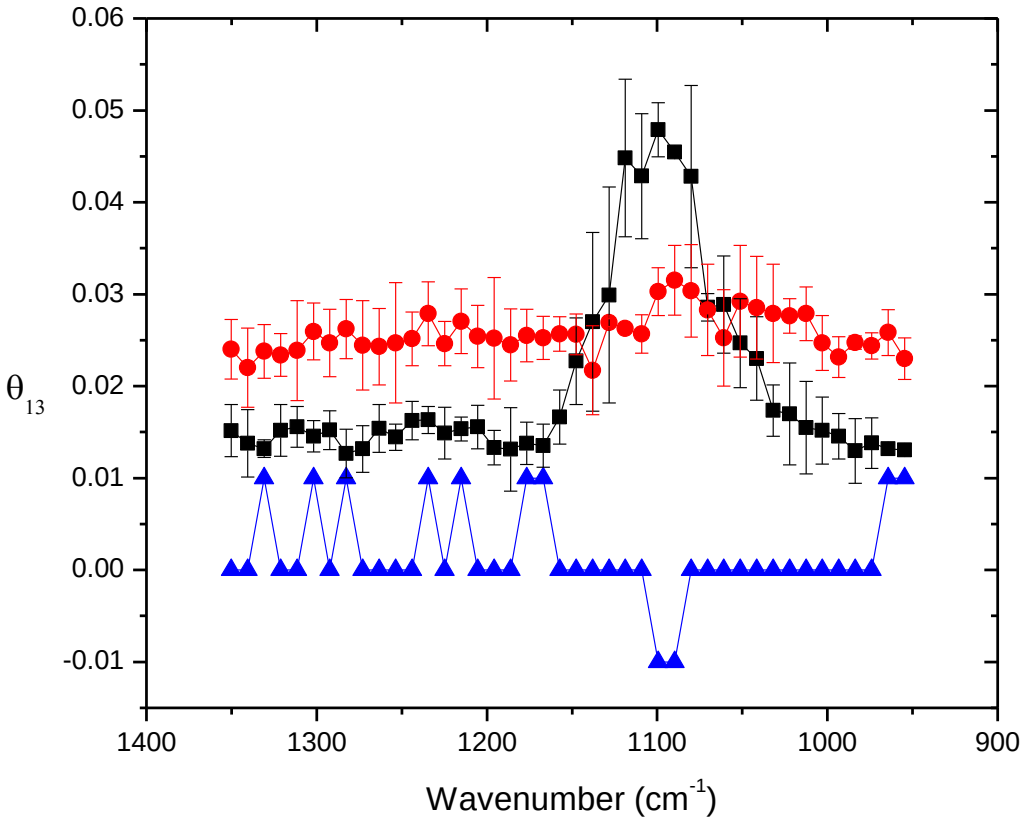

Figure 16. Effect of elevated bicarbonate levels on the model parameter $\theta_{13}(\tilde{\nu})$, the spectroscopic contribution of products in algal biomass. Positive t-test indicators (▲) depict wavenumbers at which the value for $\theta_{13}(\tilde{\nu})$ in the elevated bicarbonate sample (●) was significantly higher than the standard bicarbonate (■); a negative value indicates $\theta_{13}(\tilde{\nu})$ that is significantly lower.

Although a conclusion was reached from the results presented in this chapter, open questions remain: the observation that results for $\theta_{7,8,13}(\tilde{\nu})$ feature a high resemblance and the inconsistency and large error bars in $\theta_{9,12}(\tilde{\nu})$ indicate model insufficiencies that should be corrected by choosing an alternative modeling approach (see section 4.3). Moreover, the wavenumber-by-wavenumber approach prevented consistent values for biosediment formation across all wavenumbers, (see Figure 8D and 9D). Also, the current model made the assumption that a single two-step first-order reaction occurred at each wavenumber. The assumption of first-order reaction kinetics also limited the suitability of this model as many biologically relevant reactions, such as the reformation of DNA from two strands [95], are not first-order reactions. For these reasons, the model function was updated to facilitate a more comprehensive examination of these spectroscopic time series; recent improvements in the nonlinear regression software enabled fitting data from all wavenumbers concurrently [96].

4.3. Full Surface Modeling of Spectroscopic Time Series

An updated model function (21) was then used in an improved software version [96] and applied to the same spectroscopic time series. The first major improvement to the model function was an adjustment of the portion that described changes in spectroscopic contribution of chemical species over time, $\varepsilon(\tilde{\nu}, t)$, which led to the updated model equation (21) [96]:

$$
\begin{aligned}
Y(\tilde{\nu}, t) &= A(t) \cdot \varepsilon(\tilde{\nu}, t) + \theta_{13}(\tilde{\nu}) \\
&= \left[\theta_1 - \theta_2 \cdot \left\{1 + \theta_3 \cdot \exp\{\theta_4 \cdot (t - \theta_5)\}\right\}^{-\theta_6}\right] \\
&\cdot \left[\theta_8(\tilde{\nu}) + \sum_{h=1}^{H} \theta_{9,h}(\tilde{\nu}) \cdot e^{\left(-\theta_{10,h}(\tilde{\nu}) \cdot (t - \theta_7)\right)} + \sum_{l=1}^{L} \theta_{11,l}(\tilde{\nu}) \cdot \left[1 - e^{\left(-\theta_{12,l}(\tilde{\nu}) \cdot (t - \theta_7)\right)}\right]\right] \\
&+ \theta_{13}
\end{aligned}
\qquad (21)
$$

This adjustment was made to dismiss the assumption that a single reaction occurred at each wavenumber; now, a more universal description of the decrease in spectroscopic contribution of H reactants and increase of spectroscopic contribution of L products is represented by two sets of exponential functions. Moreover, the use of generic exponential decays or increases introduced 'time constants' albeit they do not reflect a specific potentially unknowable reaction order.

Within (21), the same function was used for the formation of biosediment, so $\theta_{1\ldots6}$ retain their meanings from the initial model function. θ_7 explains the time point at which consumption of reactant and generation of product begins, $\theta_8(\tilde{\nu})$ is the spectroscopic contribution of static compounds and $\theta_{13}(\tilde{\nu})$ represents a static spectroscopic baseline drift. $\theta_{9,h}(\tilde{\nu})$ represent the spectroscopic contribution of the reactants and $\theta_{10,h}(\tilde{\nu})$ are constants that determine the rate at which the reactants decay; at $t = 0$ contribution of reactants to spectroscopic signal will be at its maximum and will equal the sum of all values of $\theta_{9,h}(\tilde{\nu})$. $\theta_{11,l}(\tilde{\nu})$ are the contributions of products and $\theta_{12,l}(\tilde{\nu})$ are constants that determine how fast the product is formed; at $t = \infty$, the contribution to measured signal of the products will be at its maximum and will simply be equal to the sum of all values for $\theta_{11,l}(\tilde{\nu})$. For this initial application of the updated model, only one species each of reactant and product was allowed and $H = L = 1$. The software that implemented the nonlinear fitting was also improved so that the entire data set was modeled in one fit. This alleviated the problems with inconsistent biosediment formation caused by the previous wavenumber-by-wavenumber approach [96]. Panel B and D of Figure 17 depict the model functions generated from nonlinear fitting of one spectroscopic time series at standard and elevated bicarbonate concentration, respectively, using the updated model function (21). These fits are of good quality; they have correlation coefficients of 0.999 and 0.996, respectively [96].

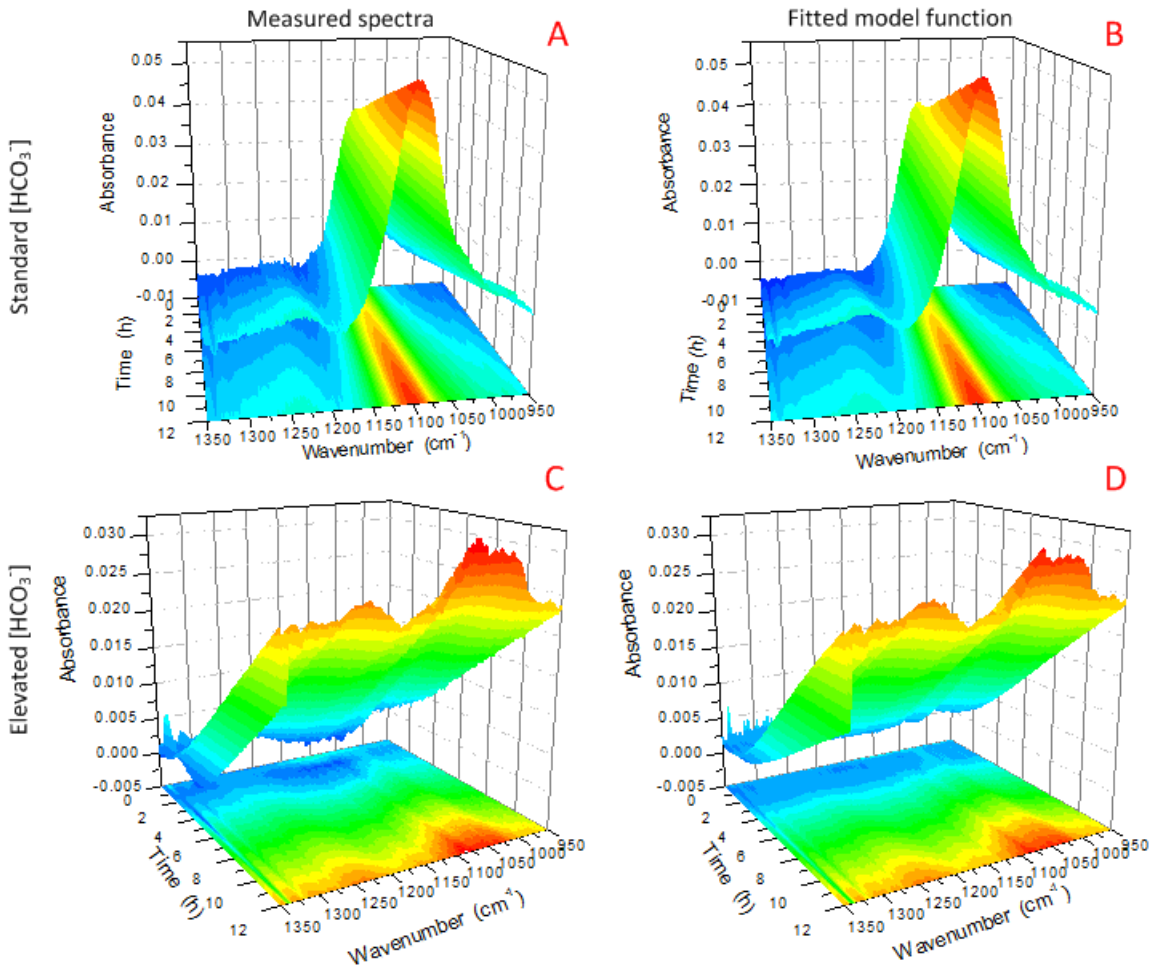

Figure 17. Two spectroscopic time series and their fitted model functions at standard (A, B), and elevated (C, D) bicarbonate concentration.

Figure 18A and B show the results for $A(t)$ obtained from the fitting of one spectroscopic time series each at standard and elevated bicarbonate concentration, respectively [96]. These two images clearly show that the improved modeling software produces values for $A(t)$ that are consistent over the entire wavenumber range, which was a large improvement over the previously applied wavenumber-by-wavenumber approach. It is clearly shown in these images that the rate at which biosediment formed was higher in the elevated bicarbonate sample. This could not be seen clearly in results for $A(t)$ obtained from use of the previous model.

Figure 18C and D depict the spectroscopic contribution of static compounds, $A(t) \cdot \varepsilon_{static}(\tilde{\nu})$ of one sample of each bicarbonate concentration [96]. Although $\varepsilon_{static}(\tilde{\nu})$ is not time dependent, the static contribution to the spectra only increases since more and more biomass $A(t)$ is accumulating over time. The contribution of static compounds is generally higher in this standard bicarbonate sample. This suggests that a certain portion of static compounds in the standard bicarbonate sample became reactants and products once the bicarbonate concentration was increased.

Figure 19A and B illustrate spectroscopic contribution of reactant $A(t) \cdot \varepsilon_{reactant}(\tilde{\nu})$ obtained from nonlinear fitting of one spectroscopic data set at each bicarbonate concentration to (21) [96]. The increased bicarbonate sample shows a higher initial contribution of reactants and a faster rate of decay at most wavenumbers. In an ideal steady-state environment there should be no reaction occurring in the biomass, which leads to little or no reactants present in the cells and $A(t) \cdot \varepsilon_{reactant}(\tilde{\nu}) \approx 0$. However, some reaction does occur in the standard bicarbonate concentration samples, implying that it is not an ideal steady state environment since nutrients are being consumed during the twelve hours while FTIR spectra were recorded. The higher initial values for $A(t) \cdot \varepsilon_{reactant}(\tilde{\nu})$ and the increased rate at which they decayed in the elevated bicarbonate sample indicates that the biomass was shifted further away from a steady state and, in turn, more chemical reactions occurred.

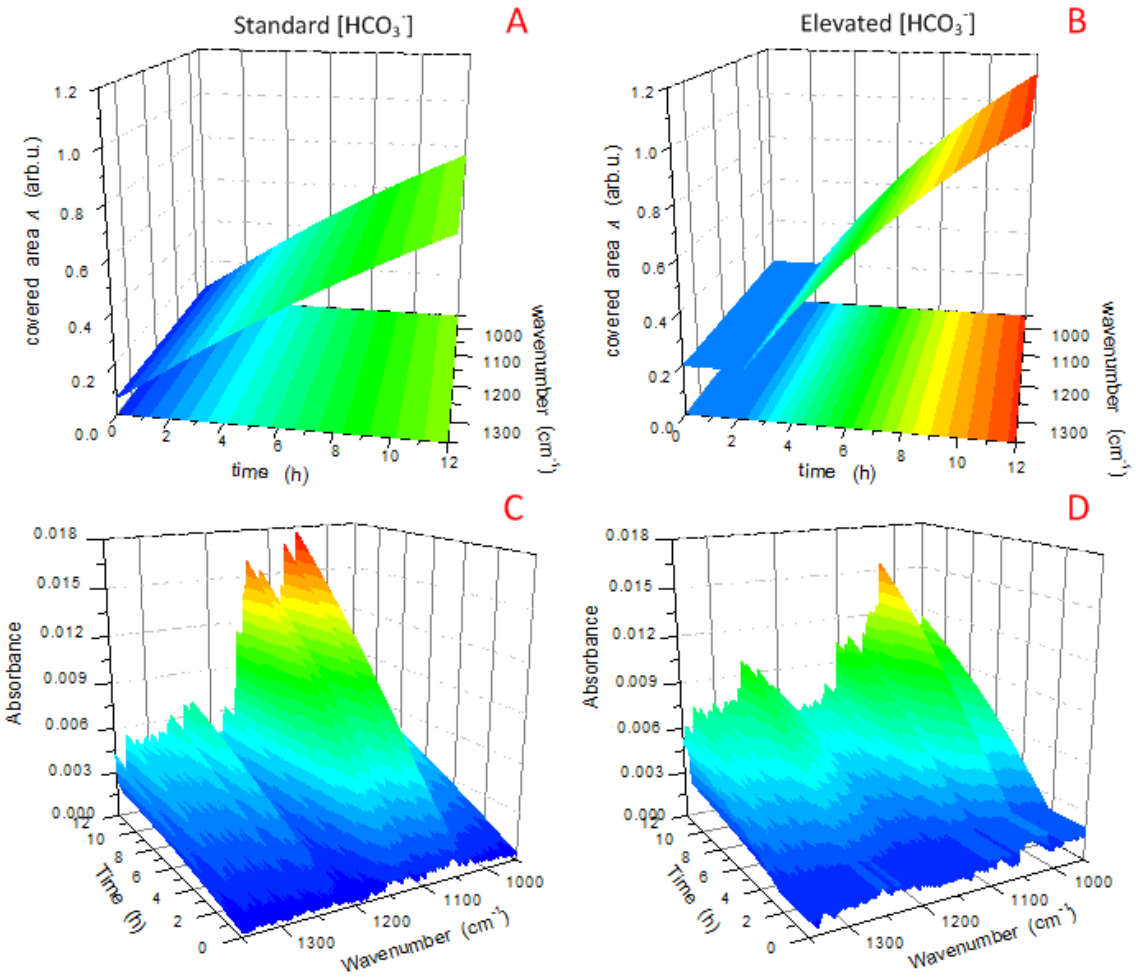

Figure 18. Buildup of biosediment $A(t)$ generated from the fitting of one spectroscopic time series each of standard (A) and elevated (B) bicarbonate concentration to the updated model function (21). Panels C and D depict the static spectroscopic contribution $A(t) \cdot \varepsilon_{static}(\tilde{\nu})$ generated from the same fitting of (21) to data sets of standard and elevated bicarbonate concentration, respectively [96].

The bottom two panels of Figure 19 depict the spectroscopic contribution of products $A(t) \cdot \varepsilon_{product}(\tilde{\nu})$ derived from fitting of (21) to data sets of standard and elevated bicarbonate concentration. The spectroscopic contribution of products approximately doubled at all wavenumbers in the increased bicarbonate sample, even at wavenumbers at which $A(t) \cdot \varepsilon_{reactant}(\tilde{\nu})$ increased very little from standard to elevated bicarbonate concentration. This seemed to indicate that the reactants from which these products were formed absorbed at wavenumbers outside of this range, which would not have been a possible conclusion using the previous model function. Though preliminary, the results in Figure 18 and 19 seem to suggest that an increased bicarbonate concentration caused an increase in the rate of biosediment formation. The amount of reaction that occurred within the biosediment also seemed to increase as static compounds decreased in increased bicarbonate and more reactants and products appeared.

Figure 20 - 23 depict values for those model parameters that are part of $\varepsilon(\tilde{\nu}, t)$. Figure 20 shows the values for $\theta_8(\tilde{\nu})$, i.e. the spectroscopic contribution of static compounds. The top image features values obtained from two samples at standard bicarbonate while the bottom images is from two elevated bicarbonate samples. The values of this parameter were inconsistent and seemed to show no dependence on the bicarbonate concentration. Results from more fitted data sets could aid in showing more consistency for this parameter at each simulated environment.

Figure 21 contains values for parameters corresponding to the decay of reactant $\theta_{9,1}(\tilde{\nu})$ and $\theta_{10,1}(\tilde{\nu})$. Values for $\theta_{9,1}(\tilde{\nu})$ presented in Figure 21A and B were also inconsistent between the two bicarbonate concentrations. The results for $\theta_{10,1}(\tilde{\nu})$ (Figure 21C and D), however, showed great improvement over previously obtained results about the dynamics of reactions within the biomass (Figure 11 and 12) as they were much more consistent between each bicarbonate concentration. Furthermore, these results seem to imply that there was an increase in the rate at which reactant decayed in the elevated bicarbonate samples.

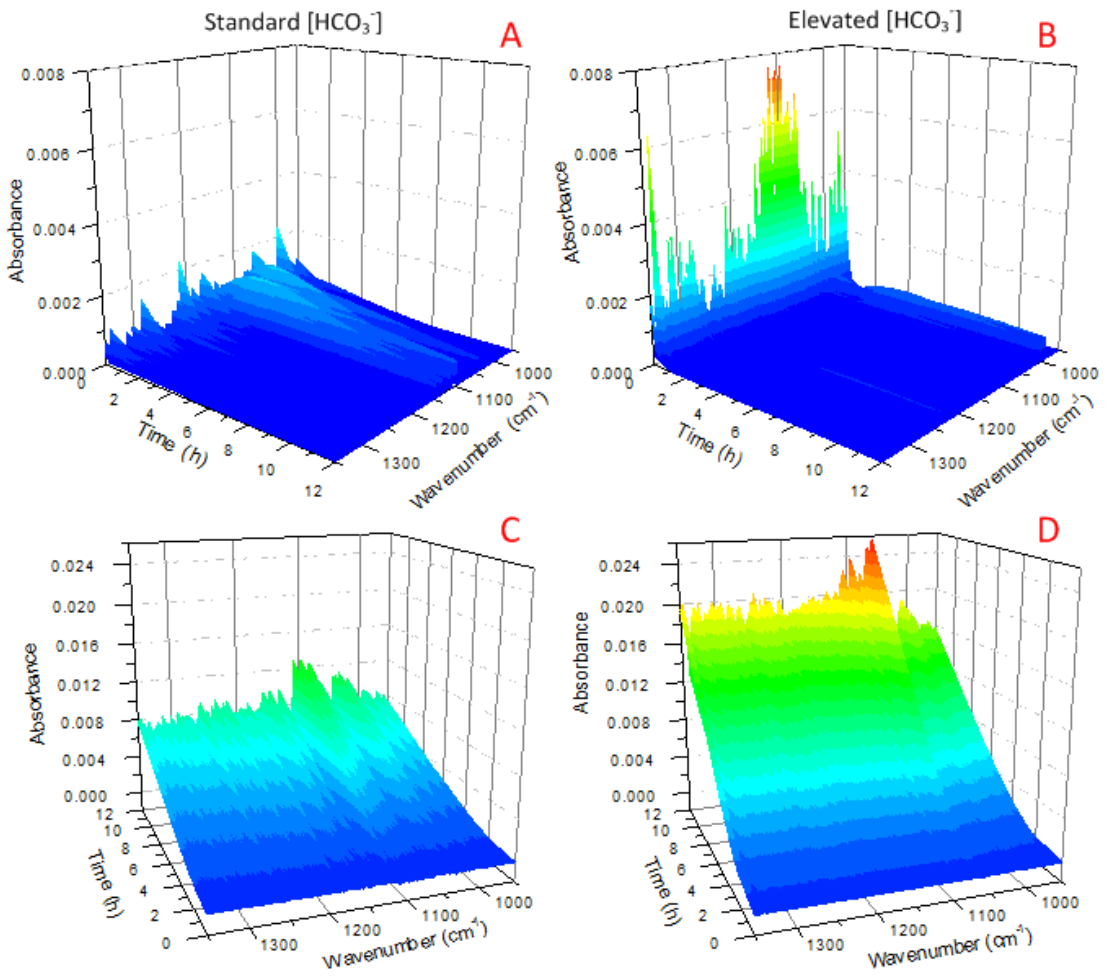

Figure 19. Spectroscopic contribution of reactant $A(t) \cdot \varepsilon_{reactant}(\tilde{\nu}, t)$ (A, B) and product $A(t) \cdot \varepsilon_{product}(\tilde{\nu}, t)$ (C, D) generated from nonlinear fitting of the improved model function (21) to one spectroscopic time series each at standard and elevated bicarbonate level [96].

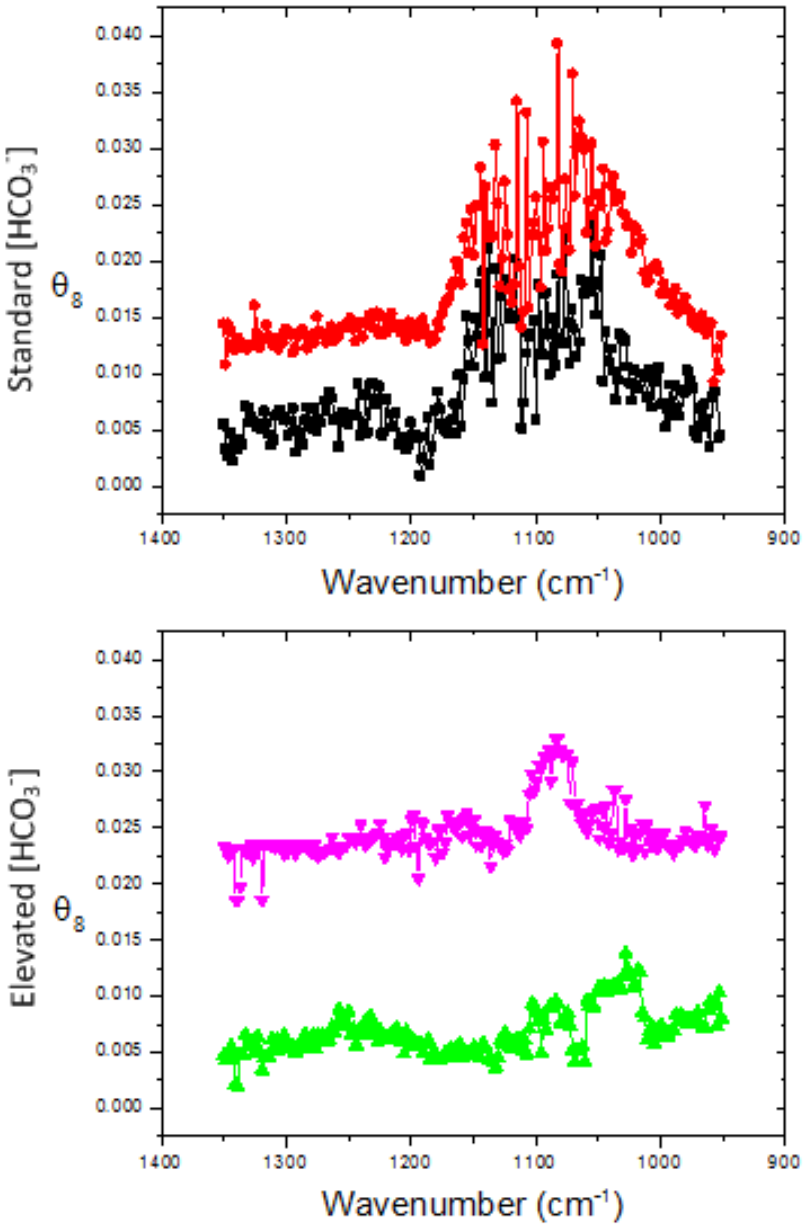

Figure 20. Spectroscopic contribution of static compounds $\theta_8(\tilde{\nu})$ generated from nonlinear fitting of updated model function (21) to two spectroscopic time series at standard (top) and elevated (bottom) bicarbonate concentration, respectively [96].

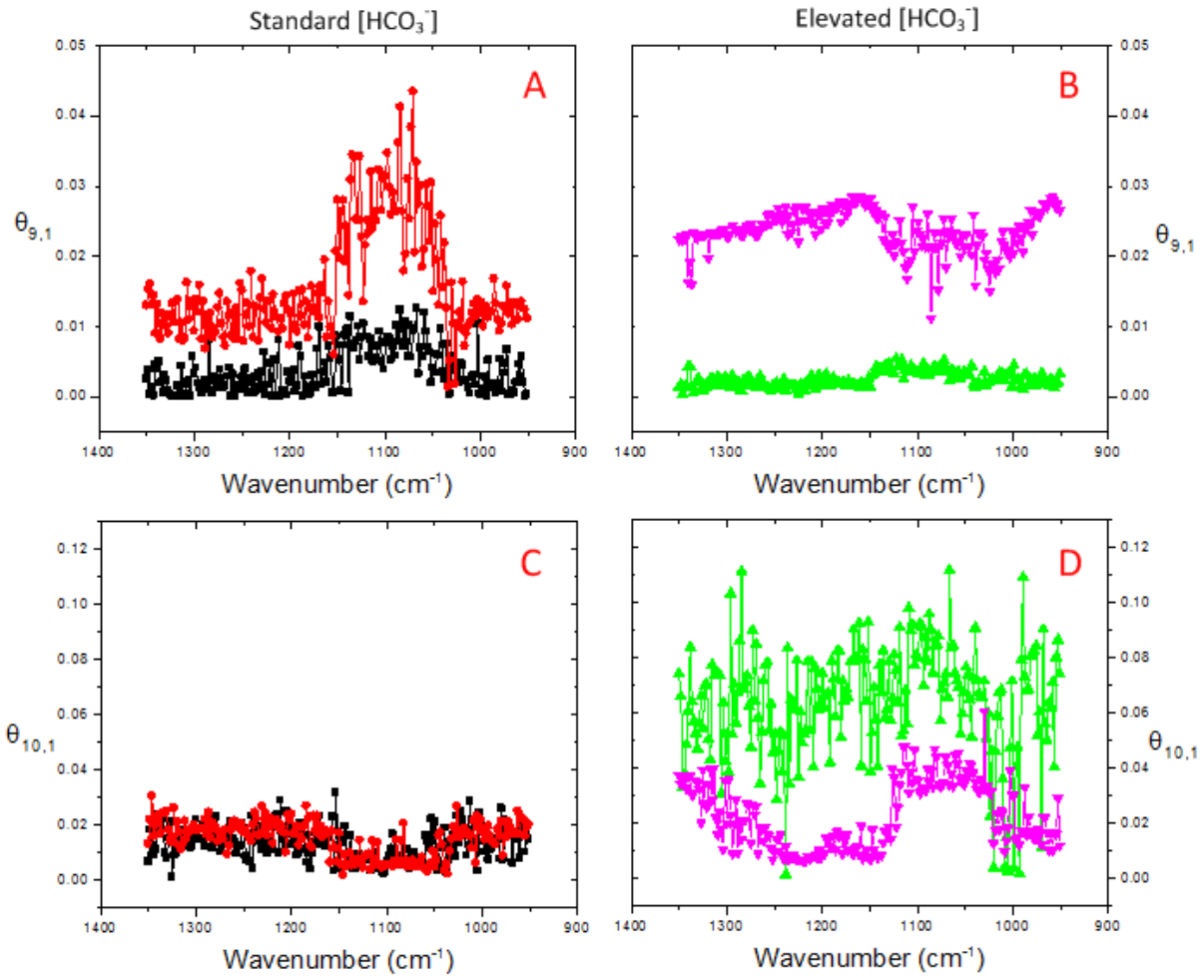

Figure 21. Model parameters for decay of reactant $\theta_{9,1}(\tilde{\nu})$ (A, B) and $\theta_{10,1}(\tilde{\nu})$ (C, D) generated from nonlinear fitting of updated model function (21) to two spectroscopic time series at standard and elevated bicarbonate concentration, respectively [96].

Figure 22 features values for $\theta_{11,1}(\tilde{\nu})$ and $\theta_{12,1}(\tilde{\nu})$, the parameters that represent how formation of product contributes to spectroscopic signal. Values for these two sets of parameters also seemed to show no dependence on increased concentration of bicarbonate. These parameters could also benefit from more available fitted data sets to show more consistency between each bicarbonate concentration. Another good improvement seen from the use of the improved model function is evident in Figure 23, where a peak at 1100 cm^{-1} is shown in the spectroscopic baseline drift; this term was often close or equal to zero in earlier results. However, this peak was not present in samples of increased bicarbonate. This also suggests that the peak seen in previous values for the spectroscopic contribution of static compounds, reactants, and products (Figure 14 - 16) was not genuine. Furthermore, it seems unlikely that increased bicarbonate caused a shift in reaction from 1100 cm^{-1} to other wavenumbers if this peak was only due to baseline shift.

Results generated from fitting to the improved model function (21) seem to suggest that although the model parameters seemed to be inconsistent, the amount of reaction in this wavenumber range seemed to increase as static compounds decreased while both the reactants and products increased due to elevated bicarbonate concentration. There also seemed to be some increase in the rate at which reactant decays and an increase in the rate at which biosediment forms. Because these results are from the fitting of only four data sets, however, it is likely that more fits to this improved model function will give a better perspective of how increased concentration of bicarbonate affects the chemistry of the algal biomass.

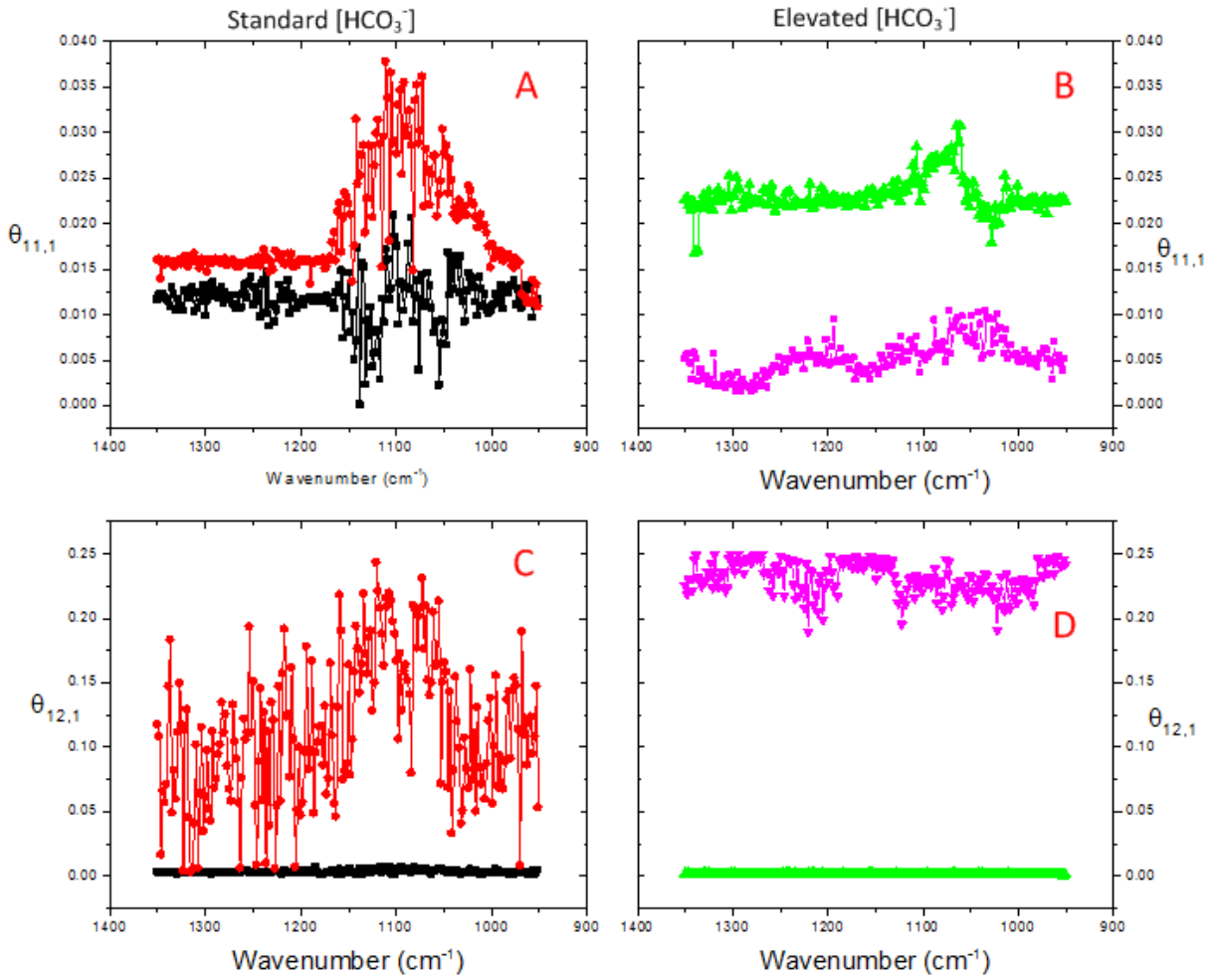

Figure 22. Model parameters from the creation of product $\theta_{11,1}(\tilde{\nu})$ (A, B) and $\theta_{12,1}(\tilde{\nu})$ (C, D) generated from nonlinear fitting of updated model function (21) to two spectroscopic time series at standard and elevated bicarbonate concentration, respectively [96].

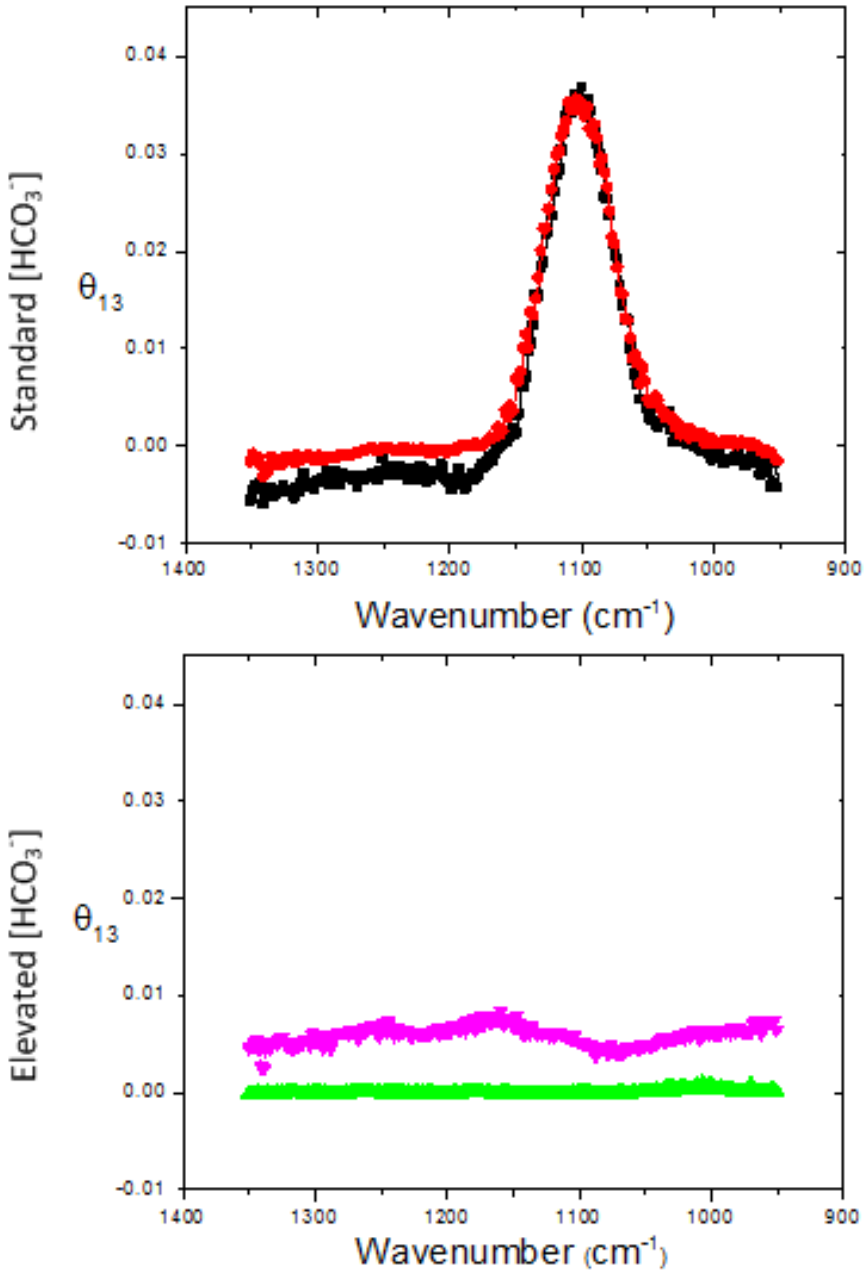

Figure 23. Spectroscopic baseline drift $\theta_{13}(\tilde{\nu})$ generated from nonlinear fitting of updated model function (21) to two spectroscopic time series at standard (top) and elevated (bottom) bicarbonate concentration, respectively [96].

4.4. Conclusions

Initial nonlinear least-squares regression was performed on three spectroscopic time series from each carbon dioxide level. These regressions were performed on a wavenumber-by-wavenumber basis for each time series. Final model functions for each wavenumber were comprised of the spectroscopic contributions of reactant, intermediate, product, static compounds, and biofilm formation. The results from these initial fits showed some promise in their ability to provide interpretable information on chemical adaptation of biomass to changes in its environment. However, this model function was not ideal and a further investigation using a revised model function was deemed necessary.

The revised modeling software included all wavenumbers into one fit, which provided consistent values for biosediment formation over the entire wavenumber range. The model function was also updated to a more universal form that dismissed the assumption of one reaction at each wavenumber by allowing multiple reactants and products to exist. The updated model clearly displayed that biosediment formation increased in the elevated bicarbonate sample. However, an inadequate number of replicate fits prevented the application of t-test analysis of $\theta_{1\ldots6}$, and the previous conclusion of an increase in the cellular growth rate s could not be confirmed.

The improved model did indicate that the large peak at 1100 cm^{-1} was actually a spectroscopic baseline shift in standard bicarbonate samples. Overall, it was found that increased bicarbonate concentration had little effect on most of the model parameters, but showed that more reaction generally occurred in this wavenumber range. This model did show that consistent values for parameters that represent rates of reaction within the biomass can be calculated; this was a large improvement over the previous approach. These results are preliminary, however, and would greatly benefit from more available fitted data sets.

5. Conclusions

5.1. Summary and Conclusion

Increasing anthropogenic pollution has become a considerable problem. Marine ecosystems have been especially affected by this phenomena as agricultural and industrial runoff and excess atmospheric carbon dioxide accumulates in bodies of water. Within these marine ecosystems are many species of microalgae, which utilize these nutrients and convert them to biomass, which then serves as the basis of many aquatic food webs. It has been shown that the chemical composition of microalgae depends on the nutrient availability in their environment. Because microalgae are constantly consuming nutrient, they are constantly altering the nutrient availability in their environment; this makes the relationship that algae share with their environment complex. For this reason, further examination of this relationship will allow microalgae to serve as a link between ecology and chemistry.

Many previous examinations of microalgae were performed on dead cells, but this cannot yield any dynamic information on how microalgae adapt to their environment. For this reason, a novel culturing and experimentation technique was developed. To more closely mimic conditions algae naturally experience, cultures were prepared semicontinuously by replacing spent nutrient daily. Particular attention was given to replenishment of the bicarbonate supply by controlling the concentration of carbon dioxide in the algae's growth vessel. Once mature, cultures were subjected to twelve hours of FTIR analysis in ATR mode. This technique was made possible because of the suspended cells' tendency to sink and deposit on the ATR surface and form a biosediment. Though live cells could be sensed, the wavenumber range utilized was limited to 1350 – 950 cm^{-1} to prevent overlap with water's absorbance bands. To examine the effect of elevated bicarbonate concentration on algal samples, two groups of cultures were examined. The first group was subjected to no change in their environment when they were transferred from the growth chamber to the sample compartment; these samples served as a benchmark. The second set of samples was exposed to an elevated carbon dioxide concentration in the sample compartment.

Collected spectroscopic time series were then fitted nonlinearly to a model function that described formation of biosediment on the ATR surface and the progress of cellular reaction. This hard-modeling technique allowed interpretable chemical information to be obtained from the fitted model parameters; differences in these parameters between the two sets of algae samples could be used to explain the effect of elevated bicarbonate concentration. Initial results suggested that increased bicarbonate caused algae samples to increase their growth rate and thus shift reaction from 1100 cm^{-1} to multiple other wavenumbers within the selected wavenumber range to accommodate this increased growth rate.

However, fits to the initial model function produced inconsistent predictions of how the biosediment formed and showed no ability to discern information about the rate of reaction within the biosediment. Therefore, a further investigation of spectroscopic time series was performed using an improved model function. Though preliminary, results gained from fits to the improved model function contained consistent results for the formation of biosediment at all wavenumbers and provided some information on the rate of cellular reaction. These results also seemed to suggest that the original conclusion of a shift from 1100 cm^{-1} to other wavenumbers was incorrect and that increased bicarbonate concentration caused an increase in the formation of biosediment and the amount of reaction that occurred in this wavenumber range.

In conclusion, the initial model function was a good first step into showing that nonlinear modeling of spectroscopic time series could be successfully performed and yield interpretable chemical information about algal adaptation. Even with less available results, the updated model function seemed to show much more promise in providing relevant chemical information about microalgae.

5.2. Outlook and Future Considerations

Future experiments should aim to provide carbon dioxide to microalgae samples for the entire duration of their growth, rather than only three hours per day. The chemical model

should also account for light and dark cycles that microalgae experience daily. Originally, microalgae were to undergo FTIR analysis for twenty-four hours under a twelve hour light cycle. It was found, however, that the rate at which absorbance increased over time was higher when the light source was activated (see Appendix 1). Because the model was not designed to account for this change after light deactivation, only spectroscopic time series collected over twelve hours with constant illumination were utilized for nonlinear modeling. The change in algal activity from light to dark should be considered in future models in order to gain a more realistic picture of how algae behave in their natural environment. The relatively small wavenumber range that was utilized might also need to be expanded. Predictions about compounds that increase or decrease in concentration due to algal adaptation would have been more authentic if other bands representative of biologically relevant compounds had been available for analysis.

The next logical step for similar examinations would be to observe model parameters through a range of nutrient increases to determine any dependencies of the parameters on the concentration of this nutrient spike. Other nutrients besides bicarbonate, such as nitrate or phosphate, could also be altered. The alteration of multiple nutrients at the same time would also be a useful examination as this likely occurs in the microalgae's natural environment.

List of References

[1] T. M. L. Wigley. Climatic Change. **5**, (1983), 315-320.

[2] D. Etheddge, L. Steele, R. Langenfelds, R. Francey, J. Bm'nola, V. Morgan. Journal of Geophysical Research. **101**, (1996), 4115-4128.

[3] K. Caldeira, M. E. Wickett. Nature. **425**, (2003), 365.

[4] M. Eby, K. Zickfeld, A. Montenero, D. Archer, K. Meissner, A.Weaver. Climate. **22**, (2009), 2501-2511.

[5] J. Blunden, D. Arndt, M. Baringer (Eds.). Bulletin of the American Meteorological Society. **92**, (2011), S1–S266.

[6] http://data.giss.nasa.gov/gistemp/graphs_v3/

[7] N. C. Johnson. Nature Climate Change. **4**, (2014), 90-91.

[8] W. Cai, S. Borlace, M. Lengaigne, P. van Rensch, M. Collins, G. Vecchi, A. Timmermann, A. Santoso, M. J. McPhaden, L. Wu, M. H. England, G.Wang, E. Guilyardi, F. Jin. Nature Climate Change. **4**, (2014), 111-116.

[9] http://www.epa.gov/climatechange/science/indicators/oceans/sea-level.html

[10] J. G. Titus, V. Narayanan. Climatic Change. **33**, (1996), 151-212.

[11] H. A. Loáiciga, T. J. Pingel, El. S. Garcia. Groundwater. **50**, (2012), 37-47.

[12] R. E. Zeebe, D. Wolf-Gladrow *CO_2 in Seawater: Equilibrium, Kinetics, Isotopes* Elsivier, Amsterdam, 2001)

[13] O. Hoegh-Guldberg, P. J. Mumby, A. J. Hooten, R. S. Steneck, P. Greenfield, E. Gomez, C. D. Harvell, P. F. Sale, A. J. Edwards, K. Caldeira, N. Knowlton, C. M. Eakin, R. Iglesias-Prieto, N. Muthiga, R. H. Bradbury, A. Dubi, M. E. Hatziolos. Science. **318**, (2007), 1737-1742.

[14] K. R. N. Anthony, D. I. Kline, G. Diaz-Pulido, S. Dove, O. Hoegh-Guldberg. Proceedings of the National Academy of Sciences. **105**, (2008), 17442-17446.

[15] R. Rosa, B. A. Seibel. Proceedings of the National Academy of Sciences. **105**, (2008), 20776-20780.

[16] R. Bibby, S. Widdicombe, H. Parry, J. Spicer, R. Pipe. Aquatic Biology. **2**, (2008), 67-74.

[17] Y. Wanga, Y. Lia, F. Liua, Y. Lia, L. Songa, H. Lia, C. Menga, J. Wua. Agriculture, Ecosystems & Environment. **184**, (2014), 9-20.

[18] W.V. Reid, et al. *Ecosystem Assessment. Ecosystems and Human Well-Being: Synthesis* (Island Press, Washington D.C., 2005).

[19] R.J. Gowen, P. Tett, K. Kennington , D.K. Mills, T.M. Shammon c, B.M. Stewart, N. Greenwood, C. Flanagan, M. Devlin, A. Wither. Estuarine, Coastal and Shelf Science. **76**, (2008), 239-254.

[20] S. Yannopoulos, S. Basbas, I. Giannopoulou. Global NEST Journal. **15**, (2013), 85-92.

[21] M. Behrenfeld, K. Halsey, A. Milligan. Philosophical Transactions of the Royal Society B. **363**, (2008), 2687-2703.

[22] M. Giordano, J. Beardall, J. Raven. Annual Review of Plant Biology. **56**, (2005), 99-131.

[23] C. B. Field, M. J. Behrenfeld, J. T. Randerson, P. Falkowski. Science. **281**, (1998), 237-240.

[24] M. Giordano, M. Kansiz, P. Heraud, J. Beardall, B. Wood, D. McNaughton. Journal of Phycology. **37**, (2001), 271-279.

[25] R. Horton, M. McConico, C. Landry, T. Tran, F. Vogt. Analytica Chimica Acta. **746**, (2012), 1-14.

[26] M. McConico, R. Horton, K. Witt, F. Vogt. Journal of Chemometrics. **26**, (2012), 585–597.

[27] M. McConico, F. Vogt. Journal of Chemometrics. **27**, (2012), 217-219.

[28] J. A. Raven, M. Giordano. Current Biology. **24**, (2014), R590-R595.

[29] A. A. Ramos, J. Polle, D. Tran. J. C. Cushman, E. Jin, J. C. Varela. Alage. **26**, (2001), 3-20.

[30] A. Minoda, H. Sawada, S. Suzuki, S. Miyashita, K. Inagaki, T. Yamamoto M.Tsuzuki. Applied Microbiology and Biotechnology. **99**, (2015), 1513-1519.

[31] Bingtao Zhaoa, Yaxin Sub. Renewable and Sustainable Energy Reviews. **31**, (2014), 121-132.

[32] R. E. Lee. *Phycology*. (Cambridge University Press, New York, 1980).

[33] D. T. Flannery, M. R. Walter. Australian Journal of Earth Sciences: An International Geoscience Journal of the Geological Society of Australia. **59**, (2012), 1-11.

[34] T. Matsunaga, H. Takeyama, H. Miyashita, H. Yokouchi. Advances in Biochemical Engineering/Biotechnology. **96**, (2005), 165-188.

[35] R. A. Andersen. *Algal Culturing Techniques* (Elsevier, Burlington, 2005).

[36] Y. Chisti. Trends in Biotechnology. **26**, (2008), 126-131.

[37] J. A. V. Costa, M. Greque de Morais. Bioresource Technology. **102**, (2011), 2-9.

[38] N. Abdel-Raouf, A.A. Al-Homaidan, I.B.M. Ibraheem. Saudi Journal of Biological Sciences. **19**, (2012), 257–275.

[39] K. Maeda, M. Owada, N. Kimura, K. Omata, I. Karube. Energy Conversion and Management. **36**, (1995), 717–720.

[40] H. Takeyama, D. Takeda, K. Yazawa, A. Yamada, T. Matsunaga. Microbiology. **143**, (1997), 2725-2731.

[41] S. Guzmán, A. Gato, J. M. Calleja. Phytotherapy Research: PTR. **15**, (2001), 224-230.

[42] K. Nisizawa, H. Noda, R. Kikuchi, T. Watanabe. Hydrobiologia. **151-152**, (1987), 5-29.

[43] M. Y. Menetrez. Environmental Science & Technology. **46**, (2012), 7073-7085.

[44] R. Kolkwitz, M. Marsson. Berichte der Deutschen Botanischen Gesellschaft. **26**, (1908), 505-519.

[45] P. V. McCormick, J. Cairns Jr. Journal of Applied Phycology. **6**, (1994), 509-526.

[46] R. J. Stevenson, J. P. Smol. in: *Freshwater Algae of North America: Ecology and Classification,* (Elsivier, San Diego, 2003).

[47] R. A. Vollenweider. Memorie dell'Istituto Italiano di Idrobiologia Dott Marco de Marchi. **33**, (1976), 53-58.

[48] R. E. Carlson. Limnology and Oceanography. **22**, (1977), 361-369.

[49] J. P. Smol. in: *Chrysophyte algae: Ecology, phylogeny and development*, (Cambridge University Press, Cambridge, U.K., 1995).

[50] R. W. Battarbee, D. E. Charles, S. S. Dixit, I. Renberg. In: *The diatoms: Applications for the environmental and earth sciences*, (Cambridge University Press, Cambridge, U.K., 1999).

[51] M. Giordano, G. Bowes. Plant Physiology. **11**, (1997), 1049-1056.

[52] J.Beardall, S. Roberts, J. Millhouse. Canadian Journal of Botany. **69**, (1990), 1146-1150.

[53] J. Beardall. Plankton Research. **13**, (1991), 133-141.

[54] M. Giordano, G. Bowes. Plant Physiology. **115**, (1997), 1049-1056.

[55] M. Giordano, V. Pezzoni, R. Hell. Plant Physiology. **124**, (2000), 857-864.

[56] E. B. Young, J. Beardall. Canadian Journal of Botany. **83**, (2005), 917-928.

[57] J. Beardall, S. Roberts, J. A. Raven. Canadian Journal of Botany. **83**, (2005), 859-864.

[58] J. Beardall, S. Stojkovic, S. Larsen. Plant Ecology & Diversity. **2**, (2009), 191-205.

[59] G. Hays, A. Richardson, C. Robinson. Trends in Ecology and Evolution. **20**, (2005), 337-344.

[60] S. Liu, P. Yao, Z. Yu, D. Li, C. Deng, Y. Zhen. Journal of Ocean University of China. **13**, (2014), 941-950.

[61] M. D. Mackey, D. J. Mackey, H. W. Higgins, S. W. Wright. Marine Ecology Progress Series. **144**, (1996), 265-283.

[62] S. A. E. Johansson, T. B. Johansson. Nuclear Instruments and Methods. **137**, (1976), 473-516.

[63] Y. Iwata. Radioanalytical and Nuclear Chemistry. **2**, (2001), 343-348.

[64] Y.Y. Huang, C.M. Beal, W.W. Cai, R.S. Ruoff, E.M. Terentjev. Biotechnology and Bioengineering. **105**, (2010), 889-898.

[65] J. Murdock, D. Wetzel. Applied Spectroscopy Review. **44**, (2009) 335-361.

[66] A. Dean, J.. Pittman, D. Sigee. Spectroscopy Europe. **26**, (2014), 14-17.

[67] M. Giordano, M. Kansiz, P. Heraud, J. Beardall, B. Wood, D. McNaughton. Journal of Phycology. **37**, (2001), 271-279.

[68] K. Stehfest, J. Soepel, C. Wilhelm. Plant Physiology and Biochemistry. **43**, (2005), 717-726.

[69] A. Domenighini, M. Giordano. Journal of Phycology. **45**, (2009), 522-531.

[70] J. Erickson, N. Hashemi, J. Sullivan, A. Weidemann, F. Ligler. Analytical Chemistry. **64**, (2012), 839-850.

[71] J. Beardall, T. Berman, P. Heraud, M. O. Kadiri, B. R. Light, G. Patterson, S. Roberts, B. Sulzberger, E. Sahan, U. Uehlinger, B. Wood. Aquatic Sciences. **63**, (2001), 107-121.

[72] A. Domenighini, M. Giordano. Journal of Phycology. **45**, (2009), 522-531.

[73] M. Gilbert, R. Luttrell, D. Stout, F. Vogt. J. Chem. Educ. **85**, (2008), 135–137.

[74] I. Jolliffe, *Principal Component Analysis, 2nd ed.*, (Springer, New York, 2002).

[75] P.J. Harrison, R. E. Waters, F.J.R. Taylor, J. Phycol. **16**, (1980), 28.

[76] J.A. Berges, D.J. Franklin, J. Phycol. **37**, (2001), 1138.

[77] A. Oren, Saline Systems. **1**, (2005), 1-14.

[78] E. Schreiber, Wiss. Meeresuntersuch, N.R., **10**, (1927), 1.

[79] L. H. White, D. W. Martin, K. K. Witt, F. Vogt. Journal of Chemometrics. **28**, (2013), 448–461.

[80] F. M. Mirabella, Jr. *Practical Spectroscopy Series; Internal reflection spectroscopy: Theory and applications* (Marcel Dekker, Inc., New York, 1993)

[81] http://www.ipcc-data.org/observ/ddc_co2.html

[82] C. Fabregas, J. Herrero, R. Abalde, B. Liano, B. Cabezas. Aquaculture. **53**, (1986), 187–199.

[83] F. Vogt, L. White. Analytica Chimica Acta. **867**, (2015), 18-28.

[84] D. Haaland, E. Thomas. Analytical Chemistry. **60**, (1988), 1193–1202.

[85] M. Tennenbaum, H. Pollard, *Ordinary Differential Equations* (Dover Publications, Mineola, NY, 1985)

[86] K. A. Connors *Chemical Kinetics, the study of reaction rates in solution* (VCH Publishers, New York, 1991).

[87] F. Vogt. Journal of Chemometrics **29**, (2014), 71-79.

[88] E. Billo, *Excel for Chemists – a Comprehensive Guide, 2nd ed*., (Wiley-VCH, New York, 2001)

[89] M. Galassi, J. Davies, J. Theiler, B. Gough, G. Jungman, P. Alken, M. Booth, F. Rossi, *GNU Scientific Library Reference Manual*, *3rd ed*., (Software V1.12 Network Theory Ltd, 2009)

[90] http://ab-initio.mit.edu/wiki/index.php/NLopt

[91] F. Vogt. Anal. Chim. Acta. **797**, (2013), 20– 29.

[92] J. N. Murdock, D. L. Wetzel. Applied Spectroscopy Reviews. **44**, (2009), 335-361.

[93] S. D. Fleming, F. Vogt. Chemometrics. **29**, (2014), 139-141.

[94] Y. Azov. Applied and Environmental Microbiology. **43**, (1982), 1300-1306.

[95] P. W. Atkins, J. De Paula. *Physical Chemistry for the Life Science*, (W. H. Freeman and Company, New York, 2006).

[96] F. Vogt, R. K. Byrd. Journal of Chemometrics. Submitted.

Appendices

Appendix 1

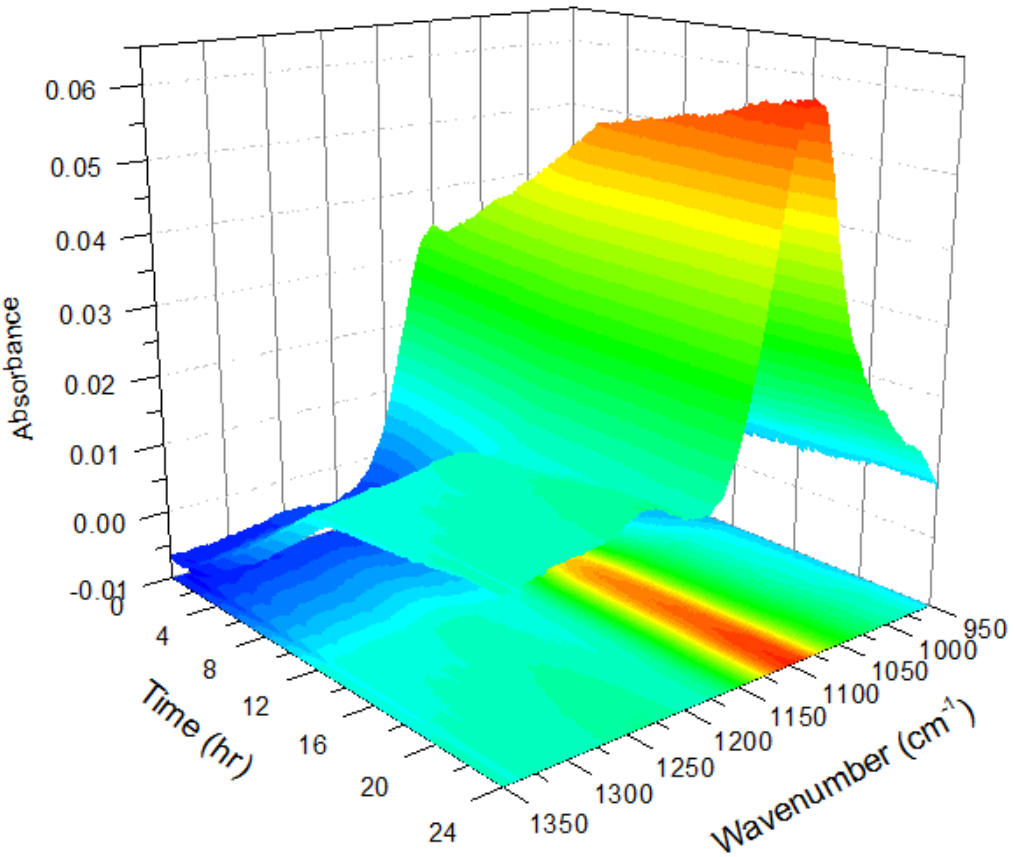

This is an example of a spectroscopic time series that was collected over twenty four hours but utilized a light cycle in which light sources were turned off after twelve hours. This caused the rate at which absorbance increased over time to visibly decrease after the light source was deactivated.

Vita

Robert Ked Byrd was born in Kingsport, TN on September 19, 1990. He was raised in Weber City, VA, attending elementary, middle, and high school in Scott County, VA. He graduated from Gate City High School in 2009 and began his undergraduate career at Emory & Henry College in the fall. Ked graduated with his B.S. in chemistry from Emory & Henry in the spring of 2013. Upon graduation, he began his graduate career in Analytical Chemistry under the direction of Dr. Frank Vogt. Ked will graduate in August 2015 with his M.S. in Analytical Chemistry where he hopes to pursue a career in chemical industry.